ORMDL3 restrains type-I interferon signaling and anti-tumor immunity by promoting RIG-I degradation

Qi Zeng [1], Chen Yao[1], Shimeng Zhang[1], Yizhi Mao[1], Jing Wang[1], Ziyang Wang [2], Chunjie Sheng[1*], Shuai Chen[1*]

[1]State Key Laboratory of Oncology in South China, Guangdong Provincial Clinical Research Center for Cancer，Sun Yat-sen University Cancer Center, Guangzhou 510060, P. R. China.

[2]Center for Translational Medicine, The First Affiliated Hospital, Sun Yat-sen University, Guangzhou, Guangdong, 510080, P.R.China.

*Correspondence to chenshuai@sysucc.org.cn (S. Chen) or shengchj@sysucc.org.cn (C. Sheng)

Abstract

Mounting evidence showed that the genetic association of ORMDL3 (ORMDL Sphingolipid Biosynthesis Regulator 3) gene polymorphisms with bronchial asthma and various inflammatory disorders. Yet its role in type I interferon (IFN) signaling remains poorly defined. Herein, we report that ORMDL3 is a negative modulator of the type I IFN signaling by engaging in an interaction with MAVS (Mitochondrial Antiviral Signaling protein) and subsequently directing RIG-I (Retinoic Acid-Inducible Gene I) for proteasome-mediated degradation. Immunoprecipitation coupled with mass spectrometry (IP-MS) assays uncovered that ORMDL3 binds to USP10 (Ubiquitin-Specific Protease 10), which forms a complex with and stabilizes RIG-I through decreasing its K48-linked ubiquitination. ORMDL3 thus disrupts the interaction between USP10 and RIG-I, thereby promoting RIG-I degradation. Additionally, subcutaneous syngeneic tumor models in C57BL/6 mice revealed that inhibition of ORMDL3 enhances anti-tumor efficacy by augmenting the proportion of cytotoxic CD8 positive T cells and IFN production in the tumor microenvironment (TME). Collectively, our findings reveal the pivotal roles of ORMDL3 in the maintenance of antiviral innate immune responses and anti-tumor immunity.

Key words: ORMDL3, IFN, RIG-I, antiviral innate immunity, anti-tumor immunity

Introduction

Type I interferons (IFN-Is) play a key role in the innate immune response to viral infections. under viral stimulations, cells produce and release interferons, which subsequently induce the transcription of interferon-stimulated genes [1,2]. Besides their critical role in antiviral immune responses, growing evidence suggests that type I interferons (IFNs) produced by malignant tumor cells or infiltrating immune cells also influence the effectiveness of cancer immunotherapies[3-5]. Many traditional chemotherapeutic drugs, targeted anti-cancer drugs, immunoadjuvants, and oncolytic viruses require intact type I IFN signaling to exert their full effects [6,7]. Furthermore, studies have shown that high intratumoral expression levels of type I IFN or IFN-stimulated genes are associated with favorable disease outcomes in cancer patients.[8]

In response to viral RNA molecules, RLRs (RIG-I-like receptors) exposed its CARD domain and then cooperate with mitochondrial antiviral signaling protein (MAVS) and TANK-binding kinase1(TBK1) to promote the production of type I interferon and transcription of different interferon-stimulated genes[9,10]. Thus, targeting RLRs can provoke anti-infection activities, moreover, RLRs also play an important role in anti-tumor immunity,for example, targeting RLRs sensitize “immune-cold” tumors to “immune hot” tumors[11]. DNA methyltransferase inhibitors facilitates upregulation of endogenous retroviruses in tumor cells, whch induce the activation of the RLR RNA recognition pathway that potentiates immune checkpoint therapy[12,13]. SB 9200, also referred to as inarigivir soproxil or GS-9992 is a dinucleotide agonist of RIG-I and nucleotide binding oligomerization domain-containing protein 2 (NOD2)[14], is in clinical trials to treat chronically infected HCV patients[15]. Another RIG-I agonist MK-4621 appears to be safe and tolerable for patients with advanced or recurrent tumors, with no dose-limiting toxicities[16].

The post-transcriptional modifications (PTMs) of RIG-I is vital for its activation and stability. Several E3-ligases have been reported for K63- or K48-linked polyubiquitination of RIG-I and regulate RLR pathway. K63-linked ubiquitination mediated by TRIM25[17] and Mex-3 RNA binding family member C (MEX3C) in CARD region of RIG-I[18,19], or mediated by RNF135 in RIG-I C-terminus[20,21], facilitates RLR signal transduction. In addition to K63 ubiquitination that usually associates with signal transduction pathways. classical degradative K48-linked polyubiquitylation also regulates RIG-I's stability. Several E3 ligases such as Cbl[22], ring finger protein 122 (RNF122)[23], RNF125[24] and TRIM40[25]. Conversely, the expression of RIG-I is also regulated by several deubiquitylating enzymes. For instance, ubiquitin specific peptidase 3 (USP3), USP21, and CYLD lysine 63 deubiquitinase (CYLD), RIG-I K63-polyubiquitin chains were removed by them and thus regulates RLR signaling pathway. [26,27], Deubiquitinase USP4 and USP15 can increase the stability of RIG-I and TRIM25 by removing K48 ubiquitination from them[28,29]. Discovering new protein machines regulating the activity or stability of RIG-I will provide new insights and targets for antiviral and anti-tumor therapies.

ORMDL3 is part of the three-member ORMDL gene family, which also includes ORMDL1 and ORMDL2. It encodes a 153-amino acid transmembrane protein that is primarily located in the endoplasmic reticulum (ER) [37]. Genetic variants in *ORMDL3* is associated with sphingolipid synthesis and altered metabolism,which contributing to asthma[30]. Recent evidence has elucidated that eosinophil trafficking, recruitment, and degranulation was regulated by ORMDL3, This regulation may contribute to the development of allergic asthma and potentially other eosinophilic disorders[31]. Additionally, ORMDL3 polymorphisms also contribute to a diverse set of inflammatory disorders that include bronchial asthma, inflammatory bowel disease[32], ankylosing

spondylitis[33], atherosclerosis[34], SLE[35] and cholangitis[36,37]. However, the role of ORMDL3 in innate immunity remains unknown.

In this study, we illuminate ORMDL3 as a pivotal negative regulator of the type I interferon (IFN) signaling pathway. ORMDL3 forms a complex with MAVS and subsequently directs RIG-I toward degradation. ORMDL3 amplifies the K48-linked ubiquitination of RIG-I by disrupting the interaction between RIG-I and UPS10. Animal experiments showed that inhibiting ORMDL3 enhances anti-tumor activity, demonstrated by an augmented proportion of activated CD8+ T cells and increased interferon production within the tumor microenvironment (TME). Collectively, our results unveil the critical role of ORMDL3 in maintaining the homeostasis of antiviral innate immune responses and suggesting ORMDL3 as a candidate target for cancer immunotherapy.

Results

ORMDL3 negatively regulates RLR induced type I IFN signaling pathway

In order to investigate the potential role of ORMDL3 in the antiviral response, HEK293T cell overexpression ORMDL3 was stimulated with polyI:C or VSV infection. The result showed that ORMDL3 significantly inhibited polyI:C and VSV stimulated transcription of *IFNB1* **(Figure 1A)**. Western blots demonstrated a marked reduction in the phosphorylation level of IRF3 when ORMDL3 was overexpressed **(Figure 1B**). Ectopic expressed ORMDL3 in A549 cells attenuated *IFNB1* expression induced by polyI:C but not polyG:C **(Figure 1C)**. This phenomenon was also observed in parallel experiments using primary mouse BMDM cells **(Figure 1D**). These findings highlight ORMDL3 as a repressor of RNA-induced type I IFN expression. To unravel the molecular mechanism underlying the suppression of type I IFN signaling by ORMDL3, luciferase

111 reporter assays were performed. ORMDL3 was found to decrease the luciferase reporter activity
112 induced by RIG-I, while showing no effect on cGAS/STING or TRIF **(Figure 1E)**. The ISRE
113 luciferase reporter assay also showed similar result **(Figure 1F)**. We constructed an ORMDL3
114 stable knockdown cell line of A549 to examine the role of ORMDL3 on viral replication. We
115 found that ORMDL3 knockdown strikingly suppressed the replication of vesicular stomatitis virus
116 (VSV), and overexpression ORMDL3 enhanced the replication of VSV **(Figure 1G)**. We also
117 infected the A549 stable knockdown cell line with herpes simplex virus-1 (HSV-1), and there is
118 no significance between shNC and shORMDL3 cell lines **(Figure 1H)**. These results suggest that
119 ORMDL3 only facilitates RNA virus replication but not DNA virus, which coincides with the
120 finding that ORMDL3 specifically represses RNA but not DNA induced type I interferon
121 expression (**Figure 1D**).

122 We next evaluated the influence of VSV, HSV-1 and RIG-I agonist SB9200 on ORMDL3
123 expression. Given the single nucleotide polymorphism (SNP) site rs7216389 at ORMDL3 locus is
124 associated with the susceptibility of childhood asthma[38] and virus-induced respiratory wheezing
125 illnesses [39], we took the genotype of this SNP into account. Upon these stimulations, HSV-1 does
126 not obviously alter the abundance of ORMDL3 **(Figure S1A)**. For VSV and SB920, the
127 expression of ORMDL3 is downregulated in some cell lines and is independent of the SNP
128 **(Figure S1B,S1C)**. Taken together, these results suggest that ORMDL3 is a negative regulator of
129 RLR RNA sensing pathway, and its expression is reciprocally repressed by this pathway.

Figure1.

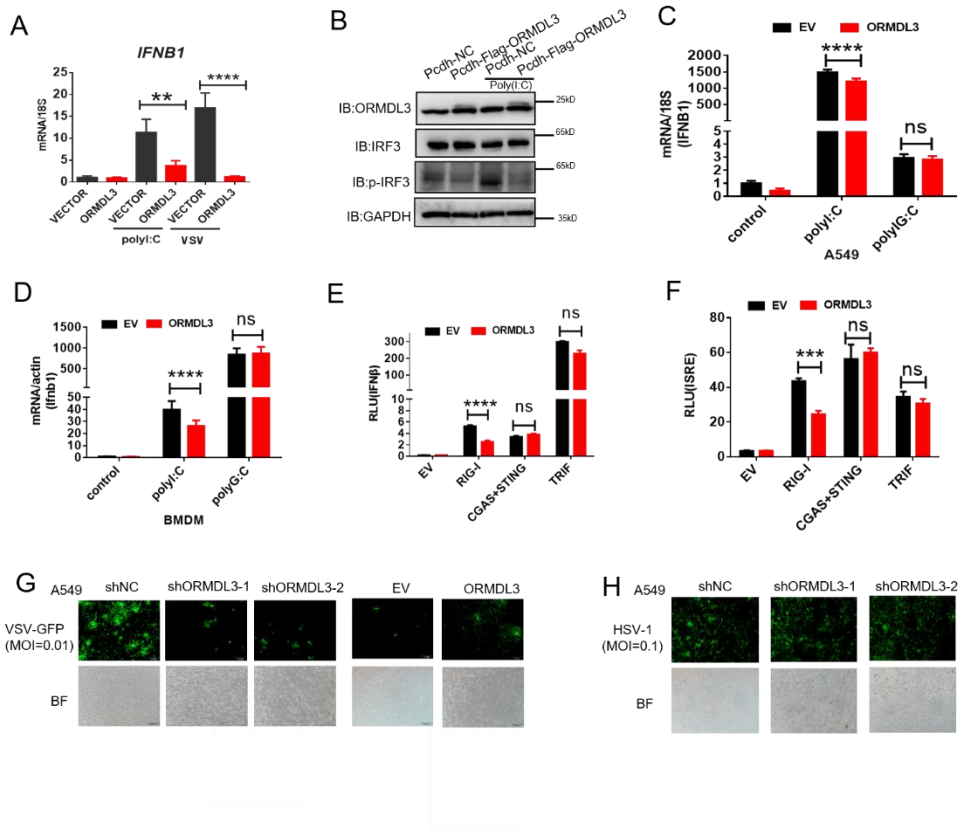

Figure 1. ORMDL3 negatively regulates RLR induced type I IFN signaling pathway.

(A) HEK293T cells were transfected with an empty vector (EV) or a ORMDL3 plasmid for 12 h and were then infected with VSV (MOI = 0.01) or transfected with polyI:C. The expression of the mRNAs encoded by the indicated genes was detected using qRT-PCR. **(B)** HEK293T -EV and HEK293T–Flag-ORMDL3 cells were transfected with or without polyI:C, and immunoblot analyses of phosphorylated IRF3 (p-IRF3), total IRF3, GAPDH and ORMDL3 levels were performed. **(C)** Results of the qRT-PCR assays showing mRNA levels of *IFNB1* in A549 cells transfected with control or ORMDL3 followed by transfected with polyI:C or polyG:C. **(D)** Results of the qRT-PCR assays showing mRNA levels of *Ifnb1* in mice primary BMDM cells infected with control or psc-AAV-ORMDL3 virus followed by transfected with polyI:C or polyG:C. **(E)** Results of the luciferase assay showing IFN-β-Luc activity in HEK293T cells

transfected with EV or ORMDL3 plasmids together with individual EV, RIG-I, cGAS plus STING, and TRIF plasmids for 24 h. **(F)** Results of the luciferase assay showing ISRE-Luc activity in HEK293T cells transfected with EV or ORMDL3 plasmids together with individual EV, RIG-I, cGAS plus STING, and TRIF plasmids for 24 h. **(G)** Wild-type and ORMDL3 stable knockdown and overexpression A549 cells were infected with VSV-GFP (MOI = 0.01) for 12 hours, and viral infectivity was detected using fluorescence microscopy. **(H)** Wild-type and ORMDL3 stable knockdown A549 cells were infected with HSV-1 (MOI = 0.1) for 24 h, and viral infectivity was detected using fluorescence microscopy. *$p < 0.05$, **$p < 0.01$, ****$p < 0.0001$. Data are representative of at least two independent experiments.

ORMDL3 regulates the protein abundance of RIG-I

Further RT-PCR results indicated that ectopic expression of ORMDL3 inhibited *IFNB1* mRNA expression and transcription of downstream genes *CCL5* and *CXCL10* induced by RIG-I and MAVS but not TBK1 or IRF3-5D **(Figure 2A,2B,S2A)**. Additionally, MDA5-induced IFN upregulation was also inhibited by ORMDL3 **(Figure S2B)**. These results revealed that ORMDL3 negatively regulates RLR pathway. Owing to ORMDL3 was down-regulated in response to VSV stimulation in HEK293T, so we firstly transfected cells with siORMDL3 followed by secondary transfection with RIG-I-N (an active form of RIG-I) in HEK293T, and we found that siORMDL3 significantly increase the expression of *IFNB1*,*CCL5* and *ISG54* **(Figure 2C)** as well as the protein abundance of RIG-I **(Figure 2D)**. Subsequent experiments involving various signaling proteins such as RIG-I (WT/N), MDA5, TBK1, and IRF3 indicated a negative correlation between ORMDL3 levels and RIG-I/RIG-I-N protein expression, with maximal degradation observed in

164 RIG-I-N **(Figure 2E)**. In addition, we also tested whether overexpressing mice Ormdl3 will also
165 lead to mice Rig-i degradation, Interestingly we discovered that mice Rig-I and human RIG-I both
166 can be degraded upon ORMDL3 overexpression, implying that ORMDL3's function is
167 conservative in human and mice (**Figure S2C,D**). In addition, ORMDL3 overexpression also
168 eliminated endogenous RIG-I protein abundance **(Figure S2E)**.

169 Based on these obervations, we focus on the relationship between RIG-I and ORMDL3. We
170 ectopically expressed an increasing amount of Flag-ORMDL3 with the RIG-I-N (harbors two
171 CARD domains) and the RIG-I-C truncated form **(Figure S2F)**, and found that ORMDL3 only
172 decreased protein abundance of RIG-I-N **(Figure 2F).** We co-transfected ORMDL3 and RIG-I
173 with or without polyI:C and found that RIG-I was degraded upon the stimulation of polyI:C,
174 suggesting that ORMDL3 degrades RIG-I only when it was activated and the CARD domain was
175 exposed **(Figure 2G)**. Further examination showed that co-expression of ORMDL3 suppressed
176 RIG-I-N induced expression of *IFNB1* and *CCL5*, as well as pro-inflammatory cytokines *IL-6* and
177 *TNF* **(Figure 2H)**, suggesting its role on both NF-κB and type I interferon pathways. Given the
178 regulation of ORMDL3 on NF-κB has been reported, we focused on its role in the type I
179 interferon pathway.

Figure 2.

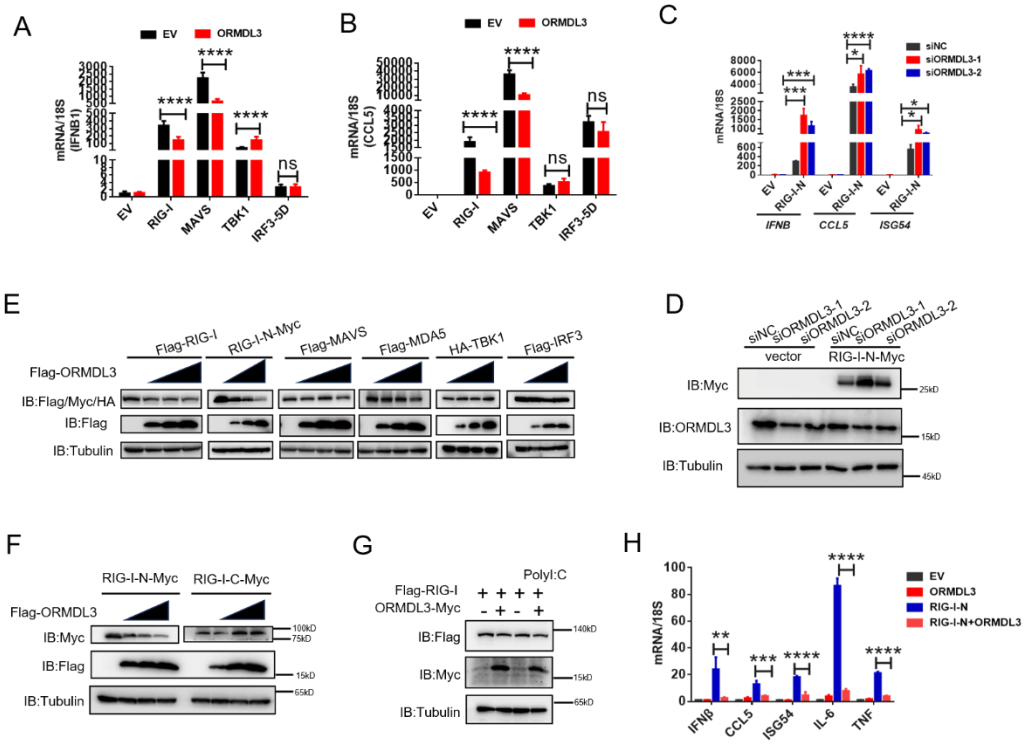

Figure 2. ORMDL3 regulates the protein abundance of RIG-I.

(A,B) RT-PCR analyses of the expression of the indicated mRNAs in HEK293T cells transfected with EV or ORMDL3 plasmids combined with co-transfection of individual plasmids encoding EV, RIG-I, MAVS, TBK1,IRF3-5D. **(C)** Results of the qRT-PCR assays showing mRNA levels of IFNB1 CCL5 and ISG54 in HEK293T cells transfected with control or ORMDL3-specific siRNAs followed by secondary transfection with EV or RIG-I-N plasmids. **(D)** Results of the WB assays show protein levels in HEK293T cells transfected with control or ORMDL3-specific siRNAs followed by secondary transfection with EV or RIG-I-N plasmids. **(E)** Immunoblot analysis of extracts of 293T cells transfected with expression vector for Flag-RIG-I,RIG-I-N-Myc and Flag-MDA5 IRF3,HA-TBK1, and increasing doses of expression vector for Flag-ORMDL3. **(F)** Immunoblot analysis of extracts of 293T cells transfected with expression vector for RIG-I-N-

Myc and RIG-I-C-Myc and increasing doses of expression vector for Flag-ORMDL3. **(G)** HEK293T cells were transfected with Flag-RIG-I and ORMDL3-Myc plasmids, as indicated, with or without polyI:C co-transfection. Cell lysates were immunoblotted with a-Flag and a-Myc antibodies. **(H)** Results of the qRT-PCR.assays showing IFNB1,CCL5,ISG54,IL-6 and TNF mRNA in HEK293T cells transfected with EV or ORMDL3 plasmids together with individual RIG-I-N plasmids for 24 h. *$p < 0.05$, **$p < 0.01$, ****$p < 0.0001$. Data are representative of at least two independent experiments.

ORMDL3 promotes the proteasome degradation of RIG-I

Two major protein degradation pathways including the ubiquitin proteasome pathway and lysosoml proteolysis system. We next identified which degradation system dominantly mediates the degradation of RIG-I by ORMDL3. We co-expressed ORMDL3 and RIG-I and treated cells with proteasome inhibitor MG132, and lysosome inhibitor CQ. We found the degradation of RIG-I mediated by ORMDL3 could be blocked by proteasome inhibitor MG132 but not lysosome inhibitor CQ **(Figure 3A)**. To rule out the possibility of transcriptional down-regulation of RIG-I, RT-PCR analysis was performed, confirming that the decrease in RIG-I protein was a post-transcriptional event **(Figure S3A)**. To investigate the mechanism, we co-transfected RIG-I-N, ORMDL3 and plasmids encoding different form of ubiquitin. The results indicated an increase in K48-linked ubiquitin chains on RIG-I-N, implicating ORMDL3 in promoting proteasomal degradation of RIG-I **(Figure 3B)**. To pinpoint the lysine residues crucial for RIG-I ubiquitination, we engineered a mutant version of RIG-I-N in which all lysines were mutated to arginines, denoted as RIG-I-N-KR. Intriguingly, the degradation-promoting effect of ORMDL3 on RIG-I-N-

214 KR was nullified **(Figure 3C)**. Given there are 18 lysine residues in RIG-I-N, we generated two
215 mutants, mutant1 and mutant2, each mutating the last nine lysines and the first nine lysines
216 **(Figure S3B)**. Remarkably, the results showed that mutant1 was resistant to degradation by
217 ORMDL3 **(Figure 3D)**, suggesting that the last nine lysines on RIG-I-N mediated its degradation
218 induced by ORMDL3.

219 To delve deeper into the intricate mechanism of ORMDL3-induced degradation of RIG-I, we
220 initially introduced single-point mutations, specifically K146R, K154R, K164R, and K172R [40],
221 which have been reported important for the function and stability of RIG-I. Co-transfection with
222 ORMDL3 revealed that these individual mutations did not impede the degradation process, hinting
223 at potential cooperation of lysine residues **(Figure 3E)**. We then mutated all four lysine residues
224 and assessed ORMDL3-induced RIG-I-N degradation. Strikingly, the RIG-I-N-4KR mutant, in
225 which K146, K154, K164, and K172 were simultaneously mutated to arginines, displayed
226 resistance to degradation by ORMDL3 **(Figure 3F)**. At the meantime, the 4KR mutant failed to
227 exhibit the upregulation of K48-linked ubiquitination induced by ORMDL3 overexpression,
228 reinforcing the pivotal role played by K146, K154, K164 and K172 in mediating RIG-I
229 ubiquitination and subsequent degradation **(Figure 3G)**. In addition, we found that in mice
230 primary BMDM when ORMDL3 was overexpressed, endogenous RIG-I was downregulated
231 **(Figure 3H)**.

Figure 3.

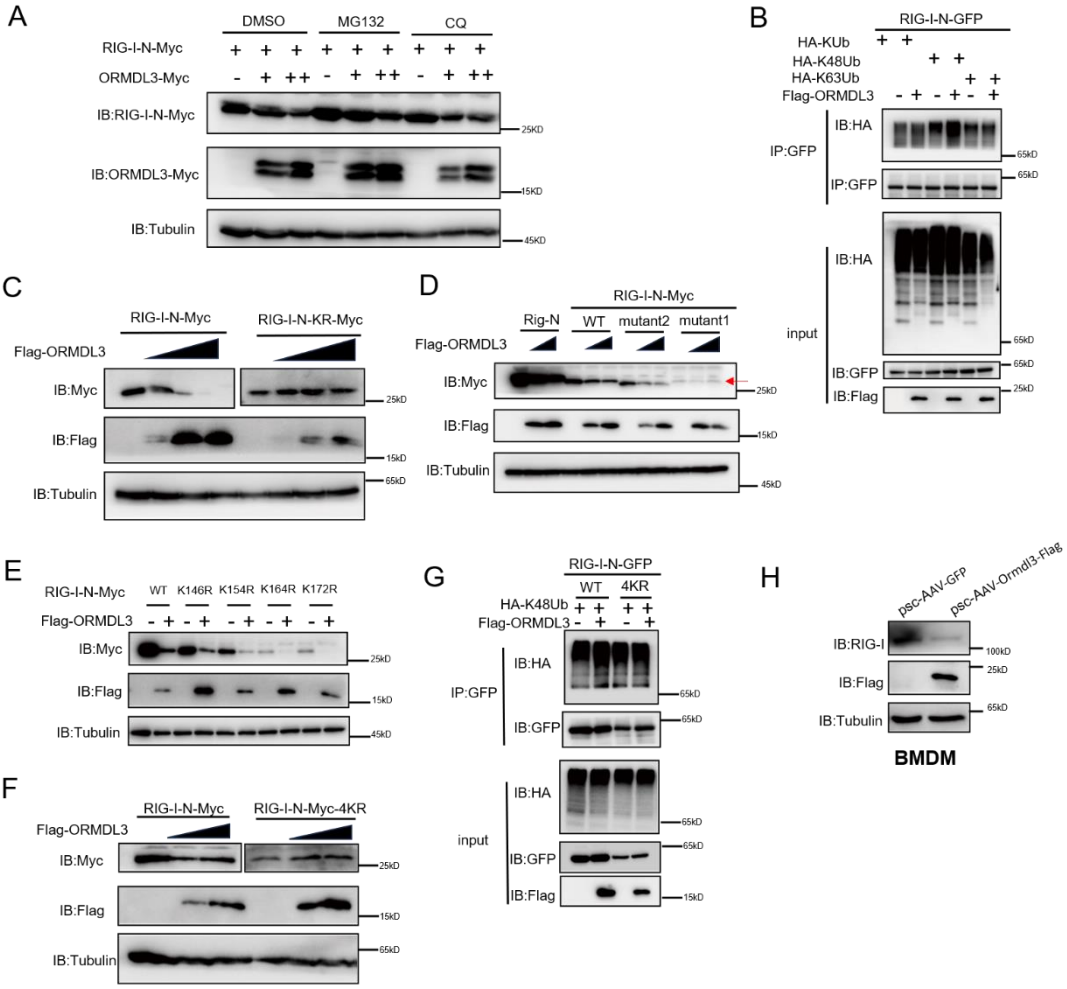

Figure 3. ORMDL3 promotes the proteasome degradation of RIG-I.

(A) HEK293T cells were transfected with plasmids encoding RIG-I-N-Myc together with increasing amounts of Flag-ORMDL3 plasmid treated with MG132 (10 μM), chloroquine (CQ) (50 μM) for 6h and the cell lysates were analyzed by immunoblot. **(B)** HEK293T cells were transfected with the indicated plasmids, and cell lysates were immunoprecipitated with an GFP antibody (a-GFP) followed by immunoblots using GFP (a-GFP) and a-HA antibodies. **(C)** 293T cells were transfected with RIG-I-N-Myc (WT or KR) and increasing doses of expression vector for Flag-ORMDL3. The expression levels of RIG-I-N-Myc were analyzed by immunoblot. **(D)**

293T cells were transfected with Rig—N,RIG-I-N-Myc (WT, KR,mutant1,mutant2), and increasing doses of expression vector for Flag-ORMDL3. The expression levels of RIG-I-N-Myc were analyzed by immunoblot. **(E)** 293T cells were transfected with RIG-I-N-Myc (WT, K146R, K154R, K164R, K172R) with or without Flag-ORMDL3. The expression levels of RIG-I-N-Myc and its mutant forms were analyzed by immunoblot**. (F)** HEK293T cells were transfected with RIG-I-N-Myc (WT or 4KR) and increasing doses of expression vector for Flag-ORMDL3. The expression levels of RIG-I-N-Myc (WT or 4KR) were analyzed by immunoblot. **(G)** HEK293T cells were transfected with RIG-I-N-GFP and HA-KUb,HA-K48Ub and HA-K63Ub with EV or Flag-ORMDL3, and cell lysates were immunoprecipitated with GFP antibody (a-GFP) followed by immunoblots using GFP (a-GFP) and a-HA antibodies. **(H)** BMDM cells were infected with psc-AAV-GFP and psc-AAV-ORMDL3-Flag virus,followed by immunoblot analysis of RIG-I, Flag and Tubulin.

ORMDL3 interacts with the signaling adaptor MAVS

Next, we sought to determine the binding partner of ORMDL3 in the type I interferon pathway. Co-immunoprecipitation(co-IP) and immunoblot analysis showed that only Flag-tagged MAVS interacted with ORMDL3-GFP **(Figure 4A)**. To delineate the requisite domains of MAVS facilitating this interaction, various MAVS truncations were co-transfected with ORMDL3. Notably, deletion of the transmembrane domain (TM) of MAVS abrogated the interaction, while deletion of the caspase activation and recruitment domain (CARD) had no discernible impact **(Figure 4B,S4A)**. It has been reported that ORMDL3 contains four TM segments (TM1−TM4) [41]. To map the essential domains of ORMDL3 that mediate its association with MAVS, we generated

264 different truncations of ORMDL3 based on the structure, which includes four truncations 1-42,
265 43-82, 83-118, 119-153 **(Figure S4B)**. Intriguingly, we found that all these four ORMDL3
266 truncations interact with MAVS **(Figure 4C)** and impede RIG-I-N induced transcription of *IFNB1*
267 and ISGs **(Figure 4D)**. In addition, co-transfection of RIG-I-N-Myc with individual ORMDL3
268 truncations showed that each domain of ORMDL3 is favorable to RIG-I-N degradation **(Figure**
269 **4E)**. Moreover, inspired by Guo et al.'s discovery of a naturally occurring short isoform of
270 ORMDL3[42], we engineered N- and C-terminal truncations of ORMDL3 to mimic this isoform
271 **(Figure S4B)**, results revealing that both truncations retained the ability to interact with MAVS
272 **(Figure S4C)**. Luciferase assays and RT-PCR affirmed the inhibitory efficacy of each domain
273 **(Figure S4D, E)**. we also tested whether these different domains can promote the degradation of
274 RIG-I-N, results revealed that every domain can amplify the degradation of RIG-I **(Figure S4F)**.
275 To further validate the association between ORMDL3 and MAVS, we did FRET experiment in
276 Hela cells, we overexpressed YFP-MAVS(donor) and CFP-ORMDL3(acceptor), when we
277 bleached YFP-MAVS, and we noticed that the fluorescence of CFP-ORMDL3 enhanced **(Figure**
278 **4F).**

Figure 4.

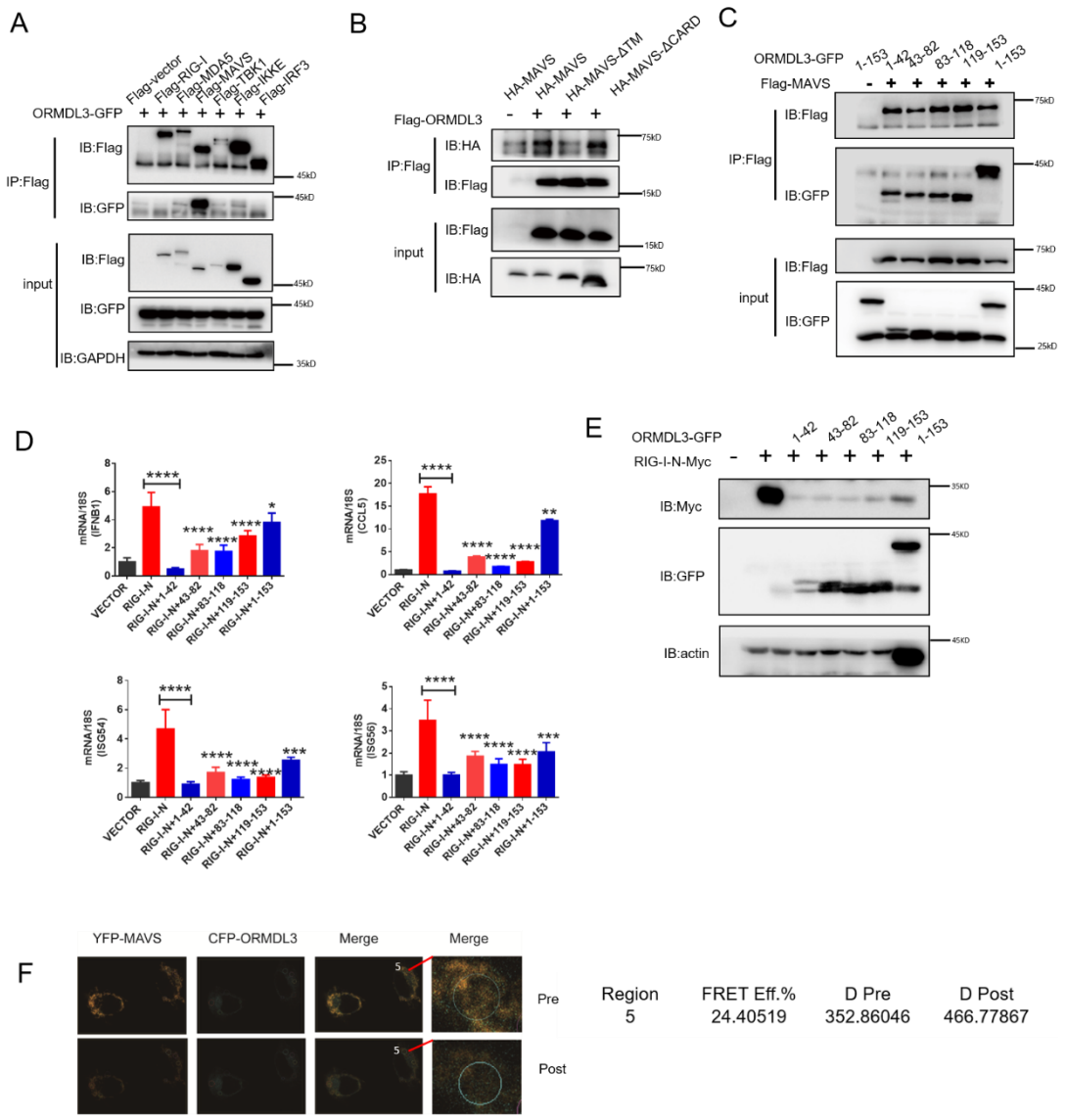

Figure 4. ORMDL3 interacts with signaling adaptor MAVS.

(A) HEK293T cells were transfected with EV or Flag-RIG-I/MAVS/MDA5/TBK1/IRF3/IKKE with ORMDL3-GFP, and cell lysates were immunoprecipitated with Flag antibody (a-Flag) followed by immunoblots using GFP (a-GFP) and a-Flag antibodies. **(B)** HEK293T cells were transfected with different MAVS truncations with EV or Flag-ORMDL3, and cell lysates were immunoprecipitated with Flag antibody (a-Flag) followed by immunoblots using HA (a-HA) and a-Flag antibodies. **(C)** HEK293T cells were transfected with EV or Flag-MAVS with different

ORMDL3 truncations, and cell lysates were immunoprecipitated with Flag antibody (a-Flag) followed by immunoblots using GFP (a-GFP) and a-Flag antibodies. **(D)** HEK293T cells were transfected with EV or Flag-MAVS with different ORMDL3 truncations, followed by RT-PCR analysis of *IFNB1*,*CCL5*,*ISG54*,*ISG56*. **(E)** HEK293T cells were transfected with RIG-I-N-Myc with EV or different ORMDL3 truncations, followed by immunoblots using GFP (a-GFP) and a-Myc antibodies. **(F)** FRET experiment of YFP-MAVS and CFP-ORMDL3 in Hela cells,YFP-MAVS is the donor and CFP-ORMDL3 is the acceptor,FRET efficiency is 24.4019%. *$p < 0.05$, **$p < 0.01$, ****$p < 0.0001$. Data are representative of at least two independent experiments.

USP10 deubiquitinates and stablizes RIG-I

To identify the E3 ligase or deubiquitinase involved in ORMDL3-mediated RIG-I ubiquitination, we conducted immunoprecipitation-mass spectrometry (IP-MS) analysis using Flag-ORMDL3 as bait and identified USP10 as a potential candidate **(Figure 5A)**. Subsequent co-IP validation demonstrated the interaction between ORMDL3 and USP10 **(Figure 5B)**, Subsequent co-IP experiment showed the interaction between USP10 and RIG-I **(Figure 5C)**. Interestingly, we found that the RIG-I level is decreased in USP10 stable knockdown 293T cells while overexpression of USP10 promotes the accumulation of RIG-I **(Figure 5D,5E)**. As USP10 is a deubiquitinase, we investigated its impact on RIG-I ubiquitination and observed a decrease in K48 ubiquitination of RIG-I upon USP10 overexpression **(Figure 5F)**. Co-expression RIG-I-N or its 4KR mutant with USP10 showed that USP10 failed to increase the RIG-I-N-4KR level, underscoring the indispensability of these residues **(Figure 5G)**. Upon overexpressing RIG-I-N and ORMDL3 in USP10 knockdown cells, ORMDL3's ability to degrade RIG-I was markedly

compromised, emphasizing the indispensable role of USP10 in this degradation process **(Figure 5H)**. This further validates that ORMDL3 disturbs the USP10's function on RIG-I.

Figure 5.

A

Gene name	-10lgP
CAND1	209.7
UFL1	68.76
* USP10	52.87
UBE3C	41.86
AMFR	47.73
UBP2L	21.73

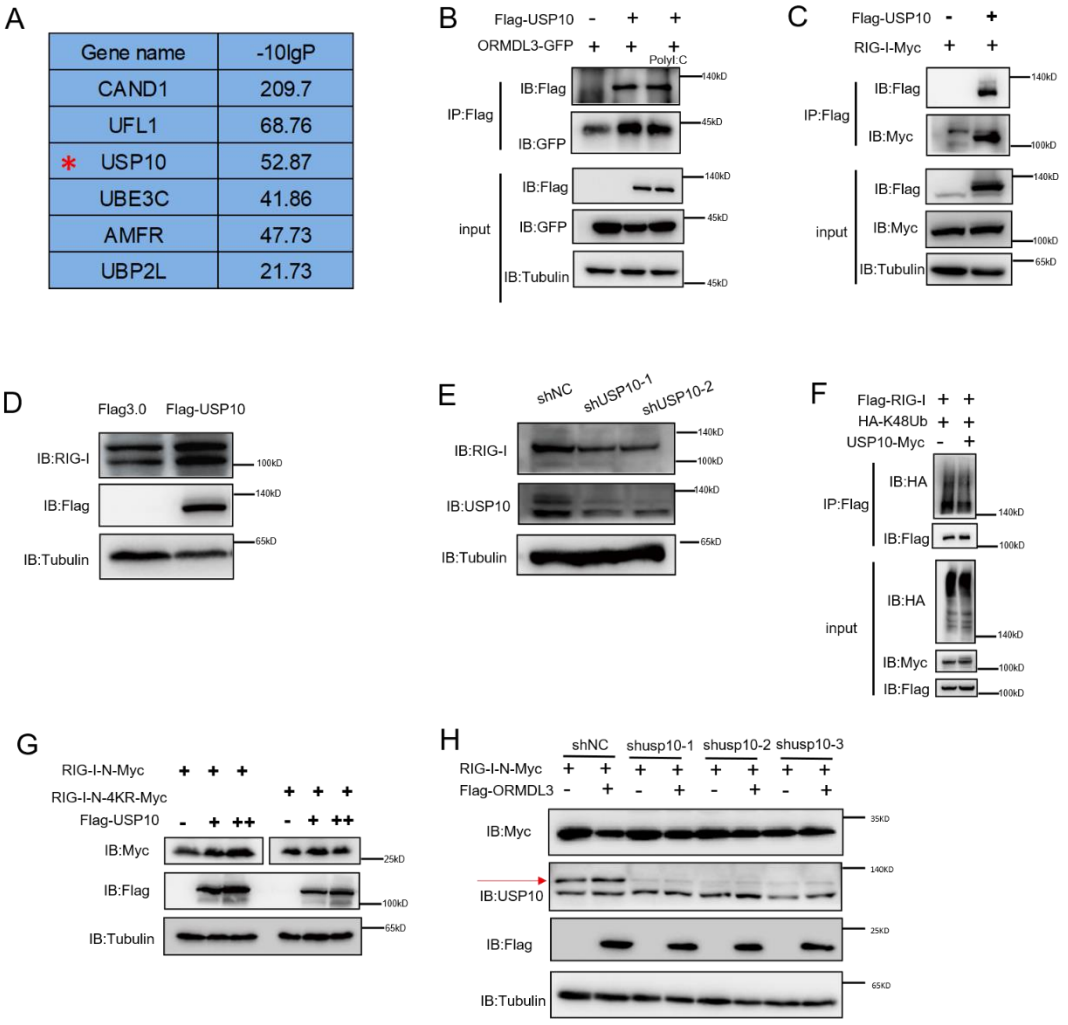

Figure 5. USP10 induces RIG-I stabilization.

(A) Protein interacted with ORMDL3 screened from mass spectrometry results. **(B)** HEK293T cells were transfected with ORMDL3-GFP and Flag-USP10 plasmids, as indicated, with or without polyI:C cotransfection. Cell lysates were immunoprecipitated with the a-Flag antibody, and immunoblotted with a-Flag and a-GFP antibodies. **(C)** HEK293T cells were transfected with RIG-I-MYC and EV or Flag-USP10 plasmids, Cell lysates were immunoprecipitated with the a-

Flag antibody, and immunoblotted with a-Flag and a-Myc antibodies**. (D)** Immunoblot the protein level of RIG-I in USP10 stable overexpression HEK293T cell line. **(E)** Immunoblot the protein level of RIG-I in USP10 stable knockdown HEK293T cell line. **(F)** IP and immunoblot analysis of 293T cells transfected with vectors expressing Flag-RIG-I and HA-K48 linked ubiquitin with or without USP10-Myc. **(G)** HEK293T cells were transfected with RIG-I-N-Myc (WT or 4KR) and increasing doses of expression vector for Flag-USP10. The expression levels of RIG-I-N-Myc were analyzed by immunoblot. **(H)** USP10 stable knockdown HEK293T cell line was transfected with RIG-I-N-Myc and Flag-ORMDL3. The expression levels of RIG-I-N-Myc were analyzed by immunoblot.

ORMDL3 disturbs USP10 induced RIG-I stabilization

Co-immunoprecipitation experiments unveiled robust interactions between USP10 and both RIG-I and ORMDL3, with ORMDL3 demonstrating the ability to disrupt the RIG-I-USP10 interaction **(Figure 6A)**. Crucially, USP10 exhibited a specific role in stabilizing RIG-I, but not other innate proteins such as MAVS, MDA5 and IRF3, and this effect can be reversed by ORMDL3 **(Figure 6B)**. Further investigations showed that the function of ORMDL3 in disturbing USP10-mediated RIG-I stabilization could be rescued by the proteasome inhibitor MG132 but not the lysosome inhibitor CQ **(Figure 6C)**. Subsequent co-transfection experiments delineated that mutations affecting all lysines (KR) or the last nine lysines (mutant1) of RIG-I-N were necessary to prevent USP10-induced accumulation and ORMDL3-mediated degradation **(Figure 6D)**. Notably, single-point mutation of the K146, K154, K164, and K172 residues on RIG-I-N does not affect the regulation of USP10 and ORMDL3 **(Figure 6E)**, while the 4KR mutation abolished this

340 process **(Figure 6F)**. These findings underscored the importance of these four lysine residues in
341 both ORMDL3-mediated degradation and USP10-stabilization of RIG-I. Building upon these
342 observations, we sought to elucidate whether USP10 stabilizes RIG-I through these four sites. Co-
343 expression of HA-K48Ub and RIG-I-N-GFP with or without USP10 revealed a decrease in K48
344 ubiquitination of RIG-I by USP10, while this effect was nullified in the presence of the 4KR
345 mutant, consistent with ORMDL3-mediated regulation **(Figure 6G)**. Additionally, we verified the
346 functional consequences of USP10-induced RIG-I stabilization by assessing the mRNA levels of
347 *IFNB1, CCL5,* and *ISG54*, which were increased upon enforced USP10 expression and reduced
348 upon co-expression with ORMDL3 **(Figure 6H)**.

Figure 6.

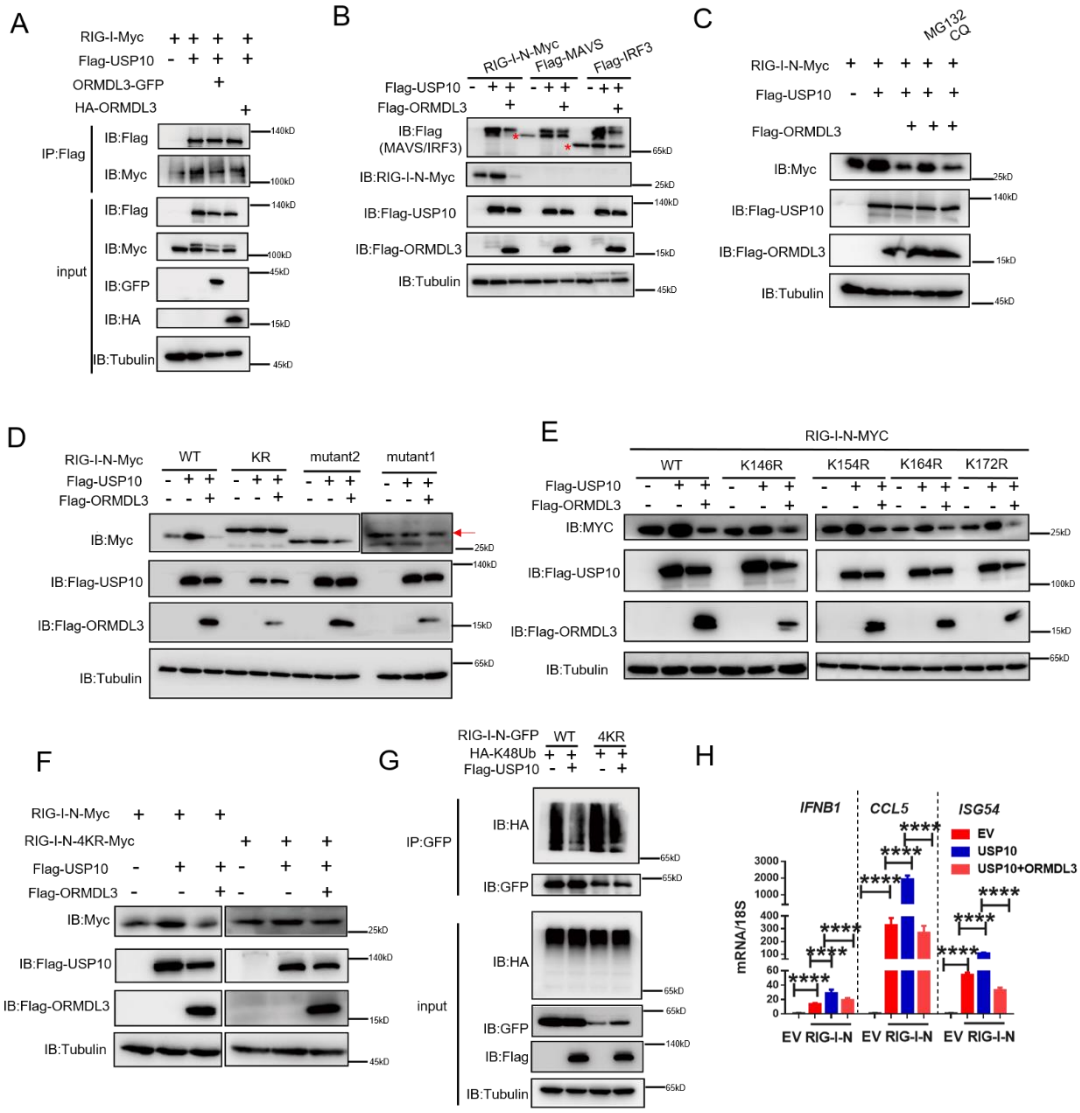

349

350 **Figure 6. ORMDL3 disturbs USP10 induced RIG-I stabilization.**

351 **(A)** HEK293T cells were transfected with Flag-USP10 and RIG-I-Myc plasmids, as indicated,

352 with or without ORMDL3 co-transfection. Cell lysates were immunoprecipitated with the a-Flag

353 antibody, and immunoblotted with a-Flag and a-Myc antibodies. **(B)** Immunoblot analysis of

354 extracts of HEK293T cells transfected with Flag-USP10 and Flag-MAVS and Flag-IRF3 and

355 RIG-I-N-Myc with or without ORMDL3 co-transfection, the cell lysates were analyzed by

356 immunoblot. **(C)** 293T cells were transfected with plasmids encoding RIG-I-N-Myc together with

Flag-USP10 with or without Flag-ORMDL3 plasmid treated with MG132 (10 μM), chloroquine (CQ) (50 μM) for 6 h The cell lysates were analyzed by immunoblot. **(D)** HEK293T cells were transfected with Flag-USP10 and RIG-I-N-Myc(WT,KR,mutant1,mutant2) plasmids, as indicated, with or without Flag-ORMDL3 co-transfection. Cell lysates were immunoblotted with a-Flag and a-Myc antibodies. **(E)** 293T cell were transfected with RIG-I-N-Myc (WT or K146R K154R K164R K172R) and Flag-USP10 with or without Flag-ORMDL3. The expression levels of RIG-I-N-Myc(WT or K146R K154R K164R K172R) were analyzed by immunoblot. **(F)** HEK293T cells were transfected with Flag-USP10 and RIG-I-N-Myc(WT and 4KR) plasmids, as indicated, with or without Flag-ORMDL3 co-transfection. Cell lysates were immunoblotted with a-Flag and a-Myc antibodies. **(G)** IP and immunoblot analysis of 293T cells transfected with vectors expressing RIG-I-N-GFP/RIG-I-N-4KR-GFP and HA-K48 Linked ubiquitin with or without USP10 transfection. **(H)** HEK293T cells were transfected with Flag-USP10 and RIG-I-N-Myc and with or without ORMDL3 co-transfection followed by RT-PCR analysis of *IFNB1*,*CCL5*.*ISG54*. *$p < 0.05$, **$p < 0.01$, ****$p < 0.0001$. Data are representative of at least two independent experiments.

Knock down of ORMDL3 enhance anti-tumor immunity

To assess the impact of ORMDL3 on anti-tumor activity, we conducted knockdown experiments targeting ORMDL3 in LLC and MC38 murine cancer cell lines, followed by subcutaneous inoculation into C57BL/6 mice. Remarkably, the deficiency of ORMDL3 significantly suppressed LCC tumor growth and reduced the tumor formation rate compared to the control group **(Figure 7A-C)**. This tumor growth inhibition by targeting ORMDL3 was further validated in the MC38 cancer model **(Figure 7G-I)**. Moreover, both in LLC and MC38 knocked

379 down cell lines, the protein level of RIG-I was significantly upregulated **(Figure S5D-G)**, and this
380 RIG-I upregulation was further verified by westernblots in LLC tumors **(Figure S5C)** and
381 immunohistochemistry (IHC) in MC38 tumors **(Figure 7K)**. Moreover, investigations revealed
382 that in the LLC tumor model, the knockdown of ORMDL3 led to a significant increase in the
383 expression of ISGs, including *CCL5, CXCL10, TNF*, and *IL-6*, compared to the control group
384 **(Figure 7D)**. This upregulation of ISGs upon ORMDL3 knockdown was consistent in the MC38
385 cancer model, where *IFNB1*, *CCL5*, and *CXCL10* mRNA levels were significantly elevated
386 **(Figure 7J)**. Flow cytometry analysis demonstrated an increase in $CD3^+$ T cell infiltration
387 percentage in LLC tumors with ORMDL3 knockdown **(Figure 7E)**. Notably, although CD8 T cell
388 levels showed no significant change among groups **(Figure S5A)**, activated CD8 T cells ($CD8^+$
389 $CD107a^+$ and $CD8^+$ $CD44^+$) exhibited a remarkable increase in the ORMDL3 knockdown group
390 **(Figure 7F,S5B)**. In addition, IHC assays revealed that more CD8 T cells were infiltrated in
391 ORMDL3 knockdown MC38 tumors **(Figure7K)**. Collectively, these findings suggest that
392 inhibition of tumor-intrinsic ORMDL3 amplifies anti-tumor immunity by increasing ISG
393 expression in the tumor microenvironment (TME) and promoting cytotoxic $CD8^+$ T cell
394 activation.

395 We further analyzed ORMDL3 expression in the TCGA-pan-cancers cohort. We observed
396 higher expression of ORMDL3 in lung adenocarcinoma (LUAD), colon adenocarcinoma
397 (COAD), and lung squamous cell carcinoma (LUSC) compared to their corresponding normal
398 samples **(Figure S6A)**. In LUAD cohorts, high ORMDL3 expression was associated with poor
399 prognosis, as indicated by overall survival (OS), progression-free survival (PFS), and disease-
400 specific survival (DSS) analyses **(Figure S6B-D)**. Analysis of LUAD cohorts also revealed

401 enrichment of stromal scores in tumors with low ORMDL3 expression**,** Additionally, we found a
402 negative correlation between ORMDL3 expression and the ESTIMATE score, indicating a
403 potential association between ORMDL3 and immune cell infiltration **(Figure S6E)**. Interestingly,
404 ORMDL3 expression showed a negative correlation with CD8 T cell activation markers such as
405 PRF1, GZMA, GZMB, as well as with ISGs such as CCL5 and CXCL10 **(Figure S6F)**, validating
406 our finding that ORMDL3 serves as a negative regulator of the IFN signaling pathway and anti-
407 tumor immunity.

Figure 7.

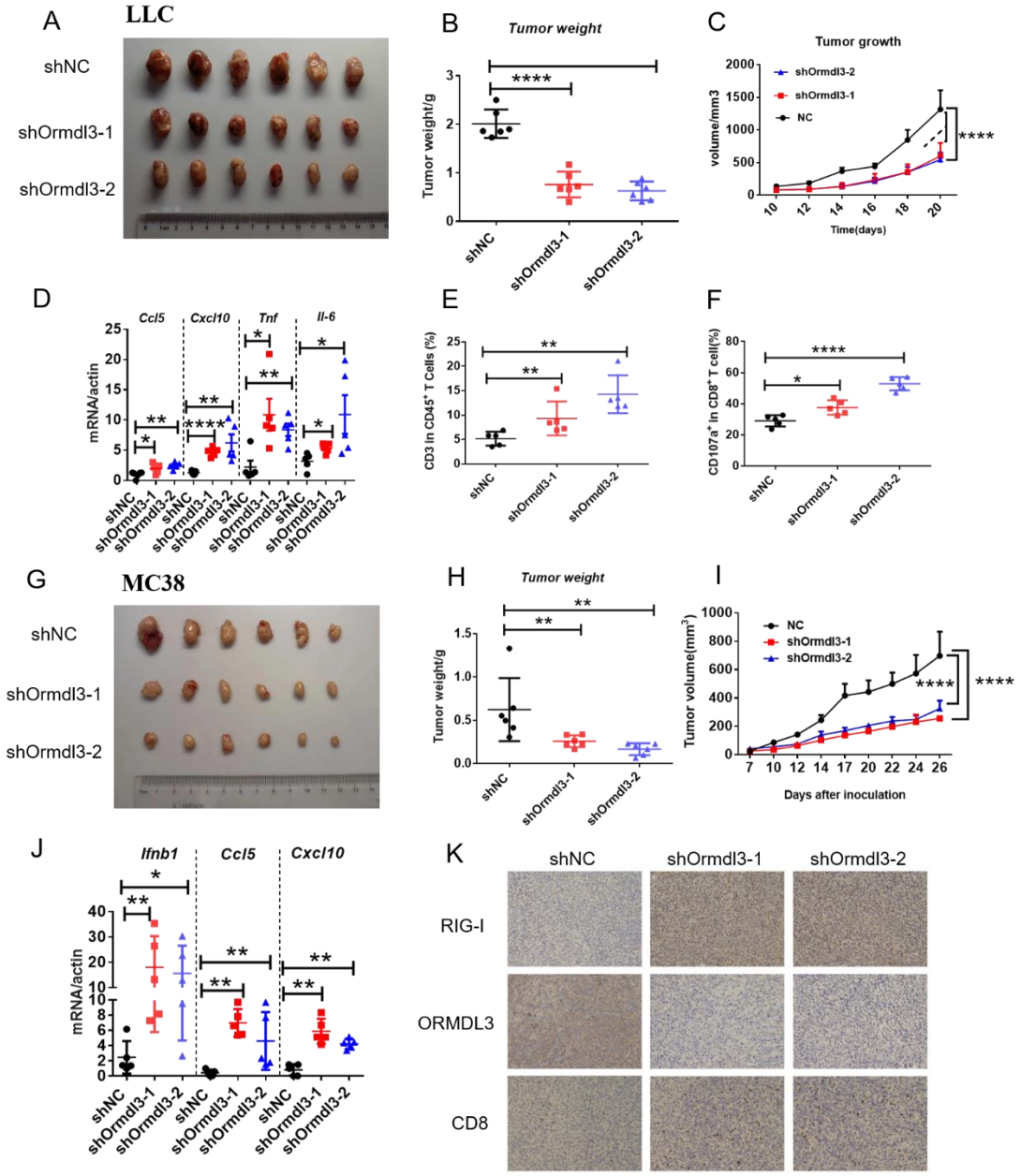

408

409 **Figure 7. Knockdown of LLC/MC38 ORMDL3 enhances anti-tumor immunity.**

410 **(A to C)** LLC tumor representative images on day 21 after tumor inoculation with shNC,

411 shORMDL3-1, shORMDL3-2 LLC stable knockdown cell line **(A)** tumor weight **(B)** tumor

412 growth **(C)** on day 21 after subcutaneous injection of 1.5×10^6LLC in C57BL/6. **(D)** Results of

413 the qRT-PCR assays showing mRNA levels of Ccl5, Cxcl10, Tnf, Il-6 of LLC tumor. **(E,F)** Flow

414 cytometry assay of CD3+ T cells in $CD45^+$, $CD107a^+$ $CD8^+$ T cells percentages. **(G to I)** MC38

415 tumor representative images on day 27 after tumor inoculation with shNC, shORMDL3-1,

416 shORMDL3-2 MC38 stable knockdown cell line **(G)** tumor weight **(H)** tumor growth **(I)** on day

417 27 after subcutaneous injection of $5\times10^{\wedge 5}$ MC38 in C57BL/6. **(J)** Results of the qRT-PCR assays

418 showing mRNA levels of Ifnb1,Ccl5.Cxcl10 of MC38 tumor. **(K)** Results of the IHC assay

419 showing expression levels of ORMDL3,RIG-I and CD8 in MC38 tumor.*$p < 0.05$, **$p < 0.01$,

420 ****$p < 0.0001$. Data are representative of at least two independent experiments.

421

422 **Discussion**

423 The RIG-I MAVS pathway is essential for the early detection of viral infections and the

424 initiation of an effective antiviral immune response, There are mainly two downstream signaling

425 events of the RIG-I MAVS pathway including interferon signaling pathway and proinflammatory

426 cytokine signaling pathway[43]. During the process of producing type I interferons, MAVS recruit

427 TBK1 amd then phosphorylate IRF3 and IRF7 and leading to the production of type I interferons.

428 And the pro-inflammatory cytokine signaling pathway mainly through the activation of NF-κB,

429 resulting in the production of pro-inflammatory cytokines, such as IL-6,TNF etc[44]. RIG-I's

430 activation is vital fo innate immunity, and its post-translational modification is important, for

431 example,TRIM25,TRIM4, RNF135,RNF194, which facilitates RIG-I activation by mediating

432 RIG-I's K63-linked ubiquitination, meanwhile ,there are also some E3 ligases mediate K48

433 ubiquitination of RIG-I, such as RNF125, RNF122, RNF55 and carboxyl terminus of HSC70-

434 interacting protein (CHIP)[45], promote its degradation through ubiquitin proteasome pathway, thus

435 attenuates cascade activation. Researchers found that some deubiquitylating enzymes also play an

436 important role in mediating RIG-I activity, for example USP3,USP21 and CYLD,they regulate
437 RIG-I activity by removing K63-linked polyubiquitin chains, In our study, we uncovered that
438 USP10 stablize RIG-I by decreasing its K48 ubiquitination on lysine 146,154,164,172.

439 Research on ORMDL3 mainly focus on exploring its relationship with asthma and its
440 exacerbations, initially,it was acknowledged that it is associated with rhinovirus infection,
441 mechanism investigation recovered that ORMDL3 regulates intercullular adhesion molecule 1
442 (ICAM1) expression and regulates ceramide and sphingolipid metabolism[30] . However, the effects
443 of ORMDL3 proteins on human innate immunity have rarely been reported. In our study, we
444 found that the mRNA level of *IFNB1* and ISGs was severely impaired in ORMDL3-
445 overexpressing cells in response to viral infection (Figure 1A) and significantly increased when
446 ORMDL3 was knocked down and co-express with RIG-I-N (Figure 2C). These data confirmed
447 that ORMDL3 acts as a negative regulator of antiviral innate immune responses. ORMDL3 is a
448 multiple transmembrane structural protein located in the center of the SPT complex, serving to
449 stabilize the SPT assembly[41]. Co-IP experiments showed that the ER protein ORMDL3 interacts
450 with mitochondrial protein MAVS, suggesting that there may exist scaffold protein to mediate
451 their interaction. ORMDL3 is reported to associate with calcium transportation[46,47], in the
452 meantime the calcium transfer between ER and mitochondria plays an important role in protein
453 synthesis, so perhaps some ERMCs proteins mediate the interaction between ORMDL3 and
454 MAVS. Furthermore, We discovered that the deubiquitinating enzyme USP10 stabilizes RIG-I and
455 ORMDL3 disturbs this process to negatively regulates IFN production. When USP10 was
456 knockdown, ORMDL3 overexpression could not facilitate RIG-I-N degradation anymore,
457 suggesting that USP10 plays an indispensable role in ORMDL3 mediating RIG-I degradation.

Collectively, we identified ORMDL3 as a negative regulator of type I interferon pathway and anti-cancer immunity. The working model is that ORMDL3 forms a complex with MAVS and promotes the degradation of RIG-I thus attenuating the transcription of type I IFN, In addition, constraining ORMDL3 can enhance IFN signaling and the proportion of cytotoxic CD8 T cell (Figure 7). The negative regulatory loop of antiviral innate immunity and anti-tumor activity involving ORMDL3 could offer insights that contribute to the development of therapeutics targeting viral infections and tumors.

Materials and Methods

Cell lines

HEK293T cell lines (from embryonic kidney of female human fetus), were cultured at 37°C under 5% CO2 in Dulbecco's modified Eagle's medium (DMEM) supplemented with 10% fetal bovine serum (ExCell, FSP500), and A549 cell lines (from lung of a 58 years old male human) were cultured in Roswell Park Memorial Institute (RPMI) 1640 medium. LLC and MC38, HCT15, DLD1, SW480, SW620 cell lines were obtained from American Type Culture Collection (ATCC) cultured in Roswell Park Memorial Institute (RPMI) 1640 medium. The cell lines used in this study have been authenticated. Mycoplasma contamination was routinely checked by PCR analysis and eliminated by treatment with PlasmocinTM (ant-mpt). The primers were as follows: Myco forward 5'- GGGAGCAAACAGGATTAGATACCCT-3'; Myco reverse 5'-GCACCATCTGTCACTCTGTTAACCTC-3'.

Viruses

VSV-GFP was provided by Prof. Rongfu Wang (Zhongshan School of Medicine, Sun Yat-sen University, China) and amplified in Vero cells. HSV-1-GFP was provided by Prof. Musheng Zeng (Sun Yat-sen University Cancer Center, China) and amplified in Vero cells. Cell lines were infected with VSV (0.01 MOI), HSV-1 (0.1MOI) for various times, as indicated in the Figures.

Plasmid and transfection

Expression plasmids for *RIG-I, MDA5, MAVS, TBK1, TRIF, IKKϵ IRF3* and *IFN-β-luc,ISRE-luc* were provided by Prof. Xin Ye (Microbiology, Chinese Academy of Sciences). Plasmid encoding *ORMDL3* was cloned in pCMV-HA/pCMV-Myc/Pcmv-flag vector, and ORMDL3 truncations ORMDL3(1-42), ORMDL3(43-82), ORMDL3(83-118) and ORMDL3(119-153) were constructed into the pEGFP-N1 vector (CLONTECH Laboratories). USP10 was obtained from prof .Tan (Sun Yat-sen University Cancer Center), and cloned into pCMV-Myc vector. For transfection of plasmids, polyI:C and polyG:C (InvivoGen) used in this study into HEK293T, A549 and BMDM cells, DNA Transfection Reagent B35101 (Bimake), PEI MW40000, pH 7.1 (Yeasen Biotechnology), Lipofectamine 2000 (ThermoFisher Scientific) or Lipofectamine 3000 (ThermoFisher Scientific) RNAimax (ThermoFisher Scientific) were used according to the manufacturer's protocol.

Flow cytometry

Single-cell suspensions were prepared from the tumor tissues of mice, Tumor tissues were cut into small pieces and washed with PBS containing 2% FBS. The tumors were digested in 15 ml RPMI supplemented with 2% FBS, 50 U/ml Collagenase Type IV(Invitrogen, California, USA), 20 U/ml

DNase (Roche, Indianapolis, IN) and incubated at 37 °C for 30min to 1 h while gently shaking. Digested tumors were then filtered through a 70 μm strainer after washed three times with PBS. Spleens were mechanically dissociated with a gentle MACS dissociator in RPMI-1640 medium supplemented with 2% FBS. Dissociated spleens were passed through a 70 μm strainer and washed three times with PBS. Red blood cells were lysed for 3 to 5 min with ACK lysis buffer and then washed with PBS containing 2% FBS. Single cells were stained with the appropriate antibodies to surface markers at 4°C for 30 minutes in the dark.The following fluorescent dye-labeled antibodies purchased from BD Biosciences, Biolegend or Invitrogen were used in this study: CD3ε-APC (145-2C11), CD4-Pacific blue (GK1.5), CD8-PE-cy7 (KT15), CD45-APC-cy7 (30-F11), CD44-FITC (IM7), CD107a-PE (1D4B). All flow cytometric data were collected on BD Fortessa X20 (BD Biosciences, San Jose, CA) and performed using Flow-Jo analysis software v10.4.while LLC tumor tissue is grinded into single cell suspension and treat as above described.

Tumor models

1×10^6 LLC tumor cells were implanted s.c. into the flanks of mice. 8×10^5 MC38 were implanted the same as LLC tumors, after the tumor was established, measure the volume of tumor once every two days.

Mass spectrometry and coimmunoprecipitation

1×10^7 HEK293T cells transfected with flag-vector or flag-ORMDL3 were prepared by washing with cold PBS and then lysed with 1× lysis buffer (Cell Signaling Technology) and incubated on ice for 30 minutes. Supernatants were collected and immunoprecipitated with the indicated

antibodies for 4 h at 4 °C, recovered by adding protein A/G Sepharose Beads (Santa Cruz Biotechnology, CA, USA, #sc-2002) overnight. After incubation, beads were washed with wash buffer and immersed in PBS then subjected to mass spectrometry. Immunoblot assays were performed with specific antibodies to identify the proteins interacting with ORMDL3. The following antibodies were used for Co-IP or immunoblot assay: ORMDL3 (abcam,107639) (abcam 211522) myc (60003-2-Ig) HA (RM1004) HA (Ray antibody) GFP (Proteintech 66002-1-Ig) and Flag (Sigma, St. Louis, USA, #F1804).

Dual-luciferase reporter assay

Cells were transfected with plasmids encoding IFN-β or ISRE luciferase reporter and RIG-I(N), MDA5, MAVS, TBK1, IRF3-5D together with pRL-TK and the plasmids encoding ORMDL3. Cells were collected and lysed 24 h post-transfection. Subsequently, the luciferase activities were measured using a Dual-luciferase Reporter Assay System (Promega, Madison, USA, #E1910). Normalization of data by the ratio of firefly luciferase activity to renal luciferase activity. Each group was measured in triplicate.

RNAi

All the siRNA oligonucleotides containing 3′dTdToverhanging sequences were chemically synthesized in genepharma (Suzhou, China) and transfected into cells using Lipofectamine ™ RNAiMAX Transfection Reagent (Thermo Fisher).The siRNAs corresponding to the target sequences were synthesized in RIBOBIO (Guangzhou, China). In this study, the siRNAs sequences were designed as follows: ORMDL3 si #1, 5′ -

GCAUCUGGCUCUCCUACGUTTdTdT 3′; ORMDL3si #2, 5′ -GGCAAGGCGAGGCUGCUAATTdTdT 3′; ORMDL3 si #3, 5′-CCCUGAUGAGCGUGCUUAUTTdTdT 3′. For transfection of siRNAs used in this study into HEK293T cells, Transfection Reagent Lipofectamine RNAiMAX (ThermoFisher Scientific) was used according to the manufacturer's protocol.

RNA extraction and quantitative real-time PCR

Total RNA from cells was extracted with Trizol reagent (Vazyme R711) according to the manufacturer's instructions. The quantity and quality of RNA were measured by Nanodrop.cDNA was synthesized using the StarScript Ⅲ All in one RT Mix with gDNA remover(Genstar). Quantitative real-time PCR was performed in a 96 well format or 384-well format on a Real-Time PCR Detection System (Bio-Rad) 2x Real Star Fast SYBR Qpcr Mix (Genstar). Relative quantification was performed with the $2^{(-\Delta\Delta CT)}$ method using 18S (for human cells) or Actb (β-Actin, for mouse cells) for normalization. The Specific qRT-PCR primers are listed in Supplementary Table 1.

Quantitative RT-PCR

Total RNA was extracted with Trizol reagent (Thermo Fisher Scientific) according to the manufacturer's instruction. Reverse-transcription products of samples were amplified by the One-step gDNA Removal and cDNA Synthesis kit (TransGen Biotech) using the SYBR Green SuperMix (Bio-Rad). Primers used for RT-PCR assays are listed in Table S1. All target gene

expression was normalized to the control gene encoding GAPDH in each individual sample and the 2-DDCt method was used to calculate relative expression changes.

Establishment of overexpressed stable cells and knock down cell lines

ORMDL3 cDNA was constructed into the pCDH-CMV-MCS-EF1 vector. A549 and HEK293T cells which stably overexpress plasmid encoding ORMDL3 were generated by lentivirus-mediated gene transfer. HEK293T cells were co-transfected with lentiviral expressing plasmid, lentiviral packaging plasmid psPAX2 (Addgene, Cat#12260) and VSV-G envelope expressing plasmid pMD2.g (Addgene, Cat#12259). After 48 hours, the lentiviruses were used for infecting A549 cells and then selected cells with puromycin (ThermoFisher Scientific). Human ORMDL3 knockdown cell line:shORMDL3 -1 and shORMDL3-2.Human USP10 knockdown cell line: shUSP10-1 and shUSP10-2, shUSP10-3.Mice Ormdl3 knockdown cell line shOrmdl3-1 and shOrmdl3-2.annealing oligos were ligated into PLKO.1 vector and after virus package infected target cell and then selected with puromycin. the shRNA sequences are listed as follows.

shORMDL3-1:

CCGGCCCACAGAATGTGATAGTAATCTCGAGATTACTATCACATTCTGTGGGTTTTTG；

shORMDL3-2：

CCGGCATGGGCATGTATATCTTCCTCTCGAGAGGAAGATATACATGCCCATGTTTTTG；

shUSP10-1:

CCGGCCTATGTGGAAACTAAGTATTCTCGAGAATACTTAGTTTCCACATAGGTTTTTG；

shUSP10-2:

CCGGCCCATGATAGACAGCTTTGTTCTCGAGAACAAAGCTGTCTATCATGGGTTTTTG；

shUSP10-3:

CCGGCGACAAGCTCTTGGAGATAAACTCGAGTTTATCTCCAAGAGCTTGTCGTTTTTG；

shOrmdl3-1:

CCGGCCAAGTATGACCAAGTCCATTCTCGAGAATGGACTTGGTCATACTTGGTTTTTG；

shOrmdl3-2:

CCGGGCCGACTTGGAGTAGCTTGTACTCGAGTACAAGCTACTCCAAGTCGGCTTTTTG.

BMDMs

Macrophages were differentiated from the bone marrow of wild-type (WT) C57BL/6 mice All bone marrow cells were flushed out and filtered through a 70-μm cell strainer. After centrifugation, red blood cells were lysed. The resultant bone marrow cells were resuspended in RPMI 1640 (Gibco) supplemented with 10% FBS (Gibco), 1% penicillin/streptomycin (Gibco), and 50 μM 2-mercaptoethanol (Sigma) in the presence of 20 ng /ml macrophage colony-stimulating factor (M-CSF; PeproTech) for 7 d. and mature BMDMs were stimulated with indicated stimulation polyI:C or polyG:C.

AAV virus production

All AAV vectors were produced in HEK293 cells via the triple plasmid transient transfection methods as pAdltea:Paav2/1:target gene=750ng:450ng:375ng. For small-scale preps, HEK293T cells were seeded in 10-cm dishes and grown to 80% confluence in Dulbecco's modified Eagle's medium (DMEM) containing 10% fetal bovine serum (FBS) (Gibco, 26140079) and 1% PenStrep (Thermo FisherScientific, 15140122). Cells were then triple transfected with the vector pscAAV-

CAG-GFP (Addgene, 83279) or pscAAV-CAG-Ormdl3, AAV1 Rep/Cap (Addgene, 112862), and Ad helper plasmid (pAddelta F6 from Addgene, 112867) at a ratio of 1:1.2:2 (3.75:4.5:7.5 μg per 10-cm dish) using PEI MW40000, pH 7.1 (Yeasen Biotechnology, 40816ES03 at a ratio 4:1 of PEI/total DNA. Cells were harvested 3 days post transfection by scraping cells off the plate in their conditioned medium and lysing cells through 3× freeze-thaw cycles between 37°C and -180°C. Preps from three replicate plates were then pooled, incubated with 25 U/mL of benzonase (Millipore Sigma, 20 E8263-25KU) at 37°C for 1 h to remove plasmid and cell DNA, centrifuged at 4°C and 1 4,000 × g for 30 min, and the supernatant filtered through a 0.22-μm polyethersulfone (PES) bottle-top filter (Corning, 431097). The filtered lysate was Purificated by iodixanol gradient ultracentrifugation. For AAV collection, the fractions obtained from the 40% phase were analyzed by measuring absorbance at 20-fold dilution at 340 nm to identify the main contaminating protein peak, as previously described. For ultrafiltration/concentrated AAV, 0.001% Pluronic F68 +200mM NaCl PBS was added to the pool to reach a total volume of 15 ml, using Amicon Ultra-15 centrifugal filter units (MWCO, 100 kDa; Merck Millipore). After concentration to a minimum of 500 μl, the product was aliquoted and stored at -80°C.

AAV titration

Prepare a plasmid stock of 2x10 molecules/μl to generate a standard curve, and then treat the puri¦ed AAV samples with DNase I to eliminate any contaminating plasmid DNA carried over from the production process (DNase does not penetrate the virion). Make 6 serial dilutions of reference sample and DNase-treated and AAV samples and detect with RT-QPCR. And then

Perform data analysis using the instrument's software. Determine the physical titer of samples (viral genomes (vg)/mL) based on the standard curve and the sample dilutions.

Immunofluorescence labeling and confocal microscopy For FRET assay

YFP-MAVS and CFP-ORMDL3 expressing plasmids were co-transfected into HeLa cells and incubated for 24h. Cells were fixed with 4% paraformaldehyde for 30 min, Images were observed on laser confocal fluorescence microscopy (Zeiss, LSM880), we bleached YFP-MAVS and measured the MFI of YFP-MAVS and CFP-ORMDL3.

Co-immunoprecipitation and immunoblot analysis

For immunoprecipitation (IP) experiments, cells were lysed with lysis buffer (Cell Signaling Technology) supplemented with protease inhibitor for 30 min. After centrifugation at 4°C, 12,000 rpm for 10 min, supernatants were collected and incubated with appropriate antibodies for 4 h and protein G beads (Santa Cruz Biotechnology) overnight. Thereafter, the beads were washed four times with cold PBS, followed by SDS-PAGE and immunoblot analysis. For immunoblot analysis, cells or tissues were lysed with RIPA buffer (Cell Signaling Technology). Protein concentrations were measured with Bradford Protein Assay Kit (Beyotime), and equal amounts of lysates were used for SDS-PAGE. The samples were eluted with SDS loading buffer by boiling for 10 min and then performed SAS-PAGE. The proteins were transferred onto PVDF membrane (Roche), and immunoblot analysis was performed with appropriated primary antibodies at 4°C overnight (Geng et al., 2017) and horseradish peroxidase (HRP) conjugated secondary anti-mouse or anti-rabbit antibodies for 1 h at room temperature. ChemiDoc Touch (Bio-Rad) achieved visualization.

Statistical analysis

The data were analyzed with GraphPad Prism 5. For two independent groups, the student's t test was used to determin statistical significance. Statistical details for individual experiments can be found in the Figure legends. Statistical significance was two-tailed and $p < 0.05$ is considered statistically significant *P value*s are indicated by asterisks in the Figures as follows: *$p < 0.05$, **$p < 0.01$, ***$p < 0.001$, and n.s. indicates non-significant.

Acknowledgements

This project was supported by grants from the Guangdong Basic and Applied Basic Research Foundation (2022A1515011930) and the National Natural Science Foundation of China (82273045).

Author Contribution

Q.Z performed most of the experiments and analyses. C.Y and Q.Z performed the mouse experiments. S.C conceived the study. C.S, S.Z, Y.M, J.W and Z.W provided technical assistance. S.C and Q.Z wrote the manuscript.

Data Availability Statement

Raw data that support the findings of this study has been deposited in Research Data Deposit database (http://www.researchdata.org.cn) with the Approval Number available upon acceptance of the manuscript. Any reasonable requests for this study are available from the corresponding author.

676 **Disclosure and competing interests statement**

677 The authors declare no competing interests.

678

679

680

681

682

683

684

685

686

687

688

689

690

691

692

693

694

695

696

697

698 **Supplementary materials**

699

700 **ORMDL3 restrains type-I interferon signaling and anti-tumor immunity by**

701 **promoting RIG-I degradation**

702

703 Qi Zeng et al.

704

705 This supplementary materials includes

706 1) Seven supplementary Figures

707 2) One supplementary Table

708

Supplementary Figure 1

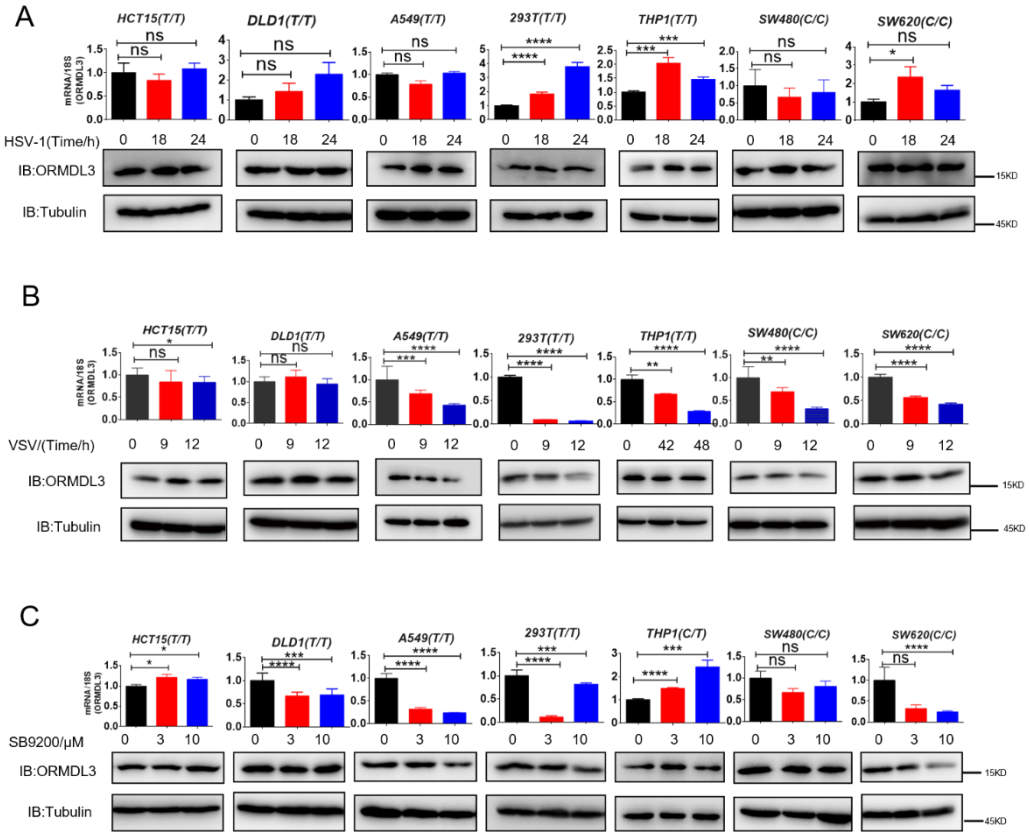

Supplementary Figure 1. ORMDL3 expression under different treatments.

(A) Results of the WB and qRT-PCR assays showing ORMDL3 protein and RNA levels HCT15 DLD1 SW480 SW620 CRC cell line and A549 293T THP1 infected with HSV (MOI = 0.1) for indicated times. **(B)** Results of the WB and qRT-PCR assays showing ORMDL3 protein and RNA levels HCT15 DLD1 SW480 SW620 CRC cell line and A549 293T THP1 infected with VSV-1 (MOI = 0.01) for indicated times. **(C)** Results of the WB and qRT-PCR assays showing ORMDL3 protein and RNA levels HCT15 DLD1 SW480 SW620 CRC cell line and A549 293T THP1 treated with RIG-I agonist SB9200 for indicated times.

Supplementary Figure 2

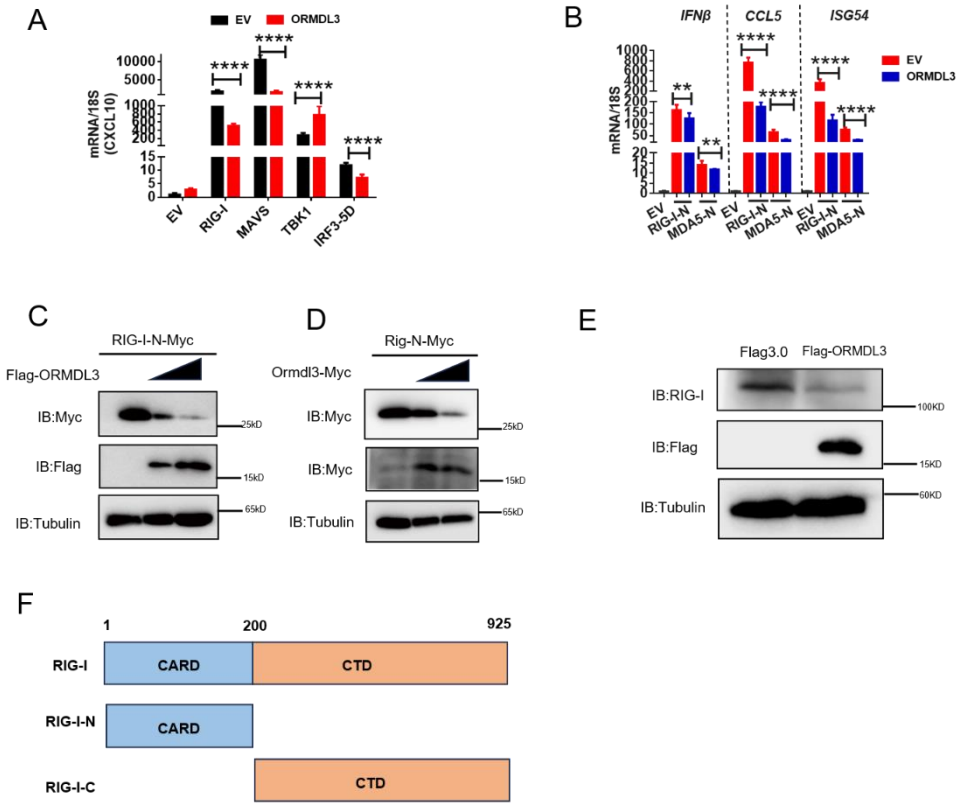

Supplementary Figure 2. ORMDL3 downregulation is conservative in both human and murine cells.

(A) RT-PCR analysis of CXCL10 when ORMDL3 was co-expressed with RIG-I MAVS TBK1 or IRF3-5D. (B) Results of the qRT-PCR.assays showing IFNB1, CCL5, ISG54 mRNA in HEK293T cells transfected with EV or ORMDL3 plasmids together with individual RIG-I-N or MDA5-N plasmids for 24 h. (C) Immunoblot assay of exogenous RIG-I expression in HEK293T transfected with ORMDL3. (D) Immunoblot assay of exogenous Rig-I expression in HEK293T transfected with Ormdl3. (E) Immunoblot assay of endogenous RIG-I expression in HEK293T transfected with ORMDL3. (F) The diagram of RIG-I truncations.

Supplementary Figure 3

A

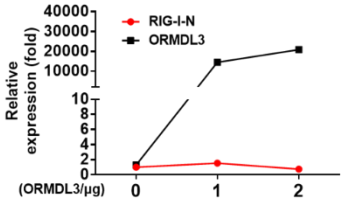

B

KRmut1 K18 K45 K48 K59 K95 K96 K99 K108 K115 K146R K154R K164R K169R K172R K177R K181R K190R K193R

KRmut2 K18R K45R K48R K59R K95R K96R K99R K108R K115R K146 K154 K164 K169 K172 K177 K181 K190 K193

4KR K18 K45 K48 K59 K95 K96 K99 K108 K115 K146R K154R K164R K169 K172R K177 K181 K190 K193

KR K18R K45R K48R K59R K95R K96R K99R K108R K115R K146R K154R K164R K169R K172R K177R K181R K190R K193R

Supplementary Figure 3. ORMDL3 promotes the degradation of RIG-I.

(A) RT-PCR assay of RIG-I-N mRNA levels in HEK293T cells transfected with RIG-I-N and increasing amounts of ORMDL3. **(B)** Different annotations of KR mutation of RIG-I-N.

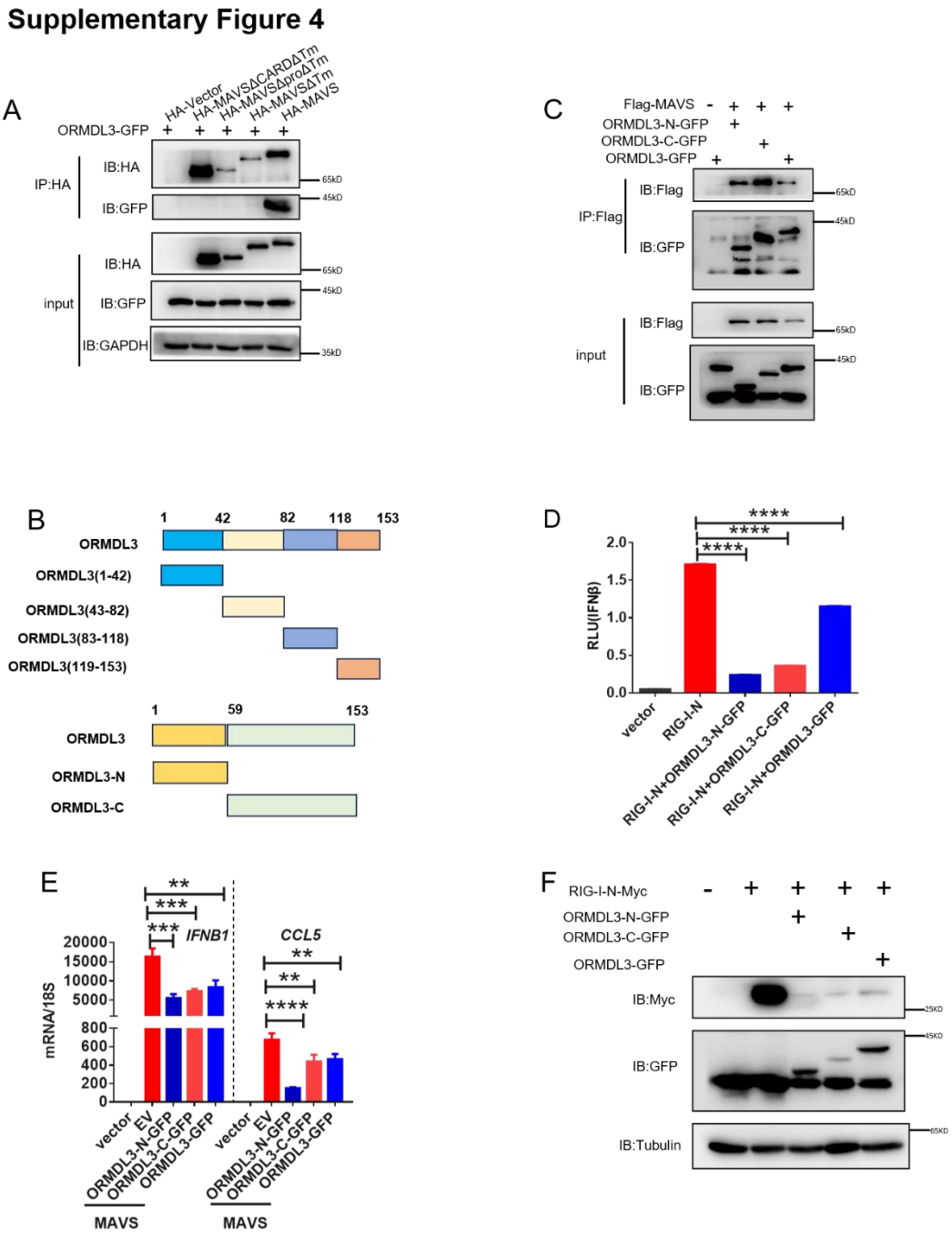

Supplementary Figure 4. ORMDL3 constrains IFN pathway by its domains.

(A) HEK293T cells were transfected with the indicated plasmids, and cell lysates were immunoprecipitated with an HA antibody (a-HA) followed by immunoblots using GFP (a-GFP) and a-HA antibodies. (B) Scheme of the truncations of ORMDL3. (C) HEK293T cells were transfected with the indicated plasmids, and cell lysates were immunoprecipitated with a Flag

antibody (a-Flag) followed by immunoblots using GFP (a-GFP) and a-Flag antibodies. (D) Results of the luciferase assays showing IFNβ activity in HEK293T cells transfected with ORMDL3 truncations with RIG-I-N. (E) Results of the qRT-PCR assays showing mRNA levels of IFNB1, CCL5 in HEK293T cells transfected with ORMDL3 truncations with MAVS. (F) HEK293T cells were transfected with RIG-I-N-Myc and different truncation of ORMDL3 and followed by immunoblot assay.

Supplementary Figure 5

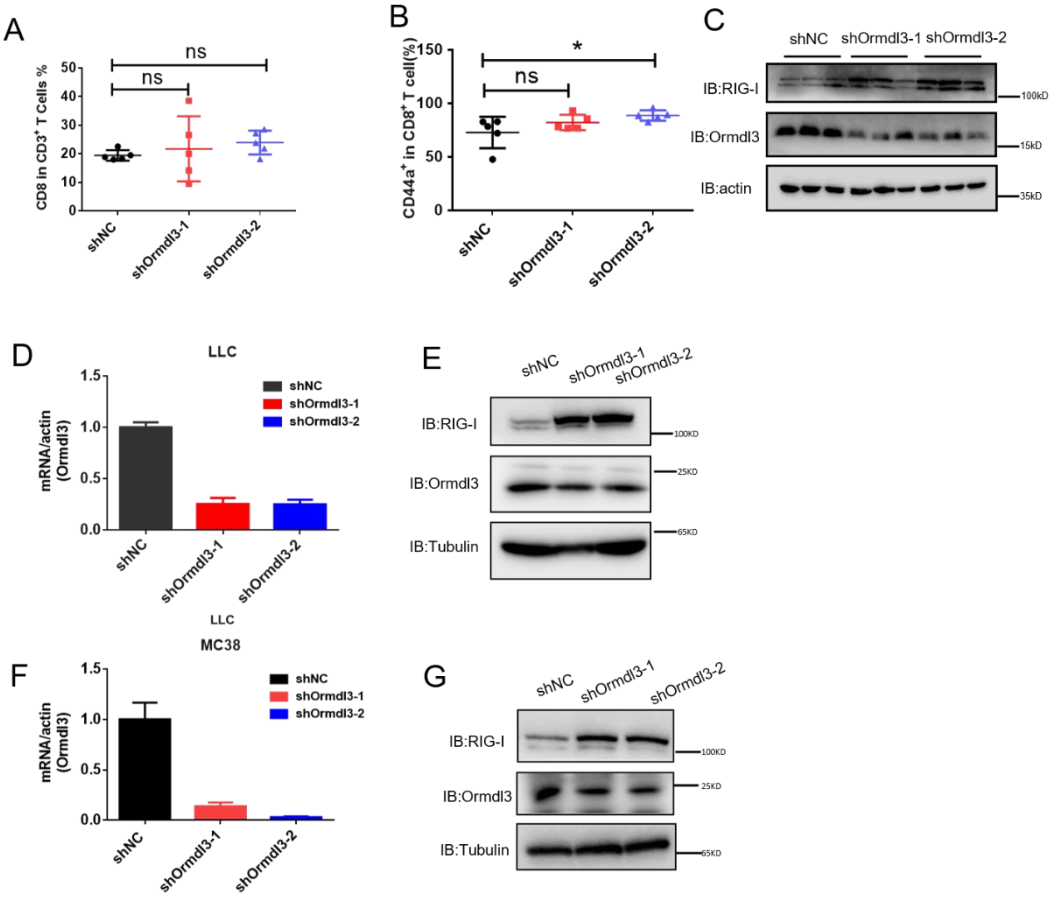

Supplementary Figure 5. Inhibiting ORMDL3 enhances the abundance of RIG-I.

(A,B) Flow cytometry assay of $CD8^+$T cells in $CD3^+$ and $CD44^+CD8^+$ T cells percentages. **(C)** Immunoblot assay of LLC tumor in group shNC, shOrmdl3-1,shOrmdl3-2, followed by analysis of protein level of ORMDL3 and RIG-I. **(D)** RT-PCR showing the shRNA knockdown of ORMDL3 or shRNA control in LLC lung cancer cells. **(E)** Immunoblot showing the shRNA knockdown of ORMDL3 or shRNA control in LLC lung cancer cells. **(F)** RT-PCR showing the shRNA knockdown of ORMDL3 or shRNA control in MC38 colon cancer cells. **(G)** Immunoblot showing the shRNA knockdown of ORMDL3 or shRNA control in MC38 colon cancer cancer cells.

Supplementary Figure 6

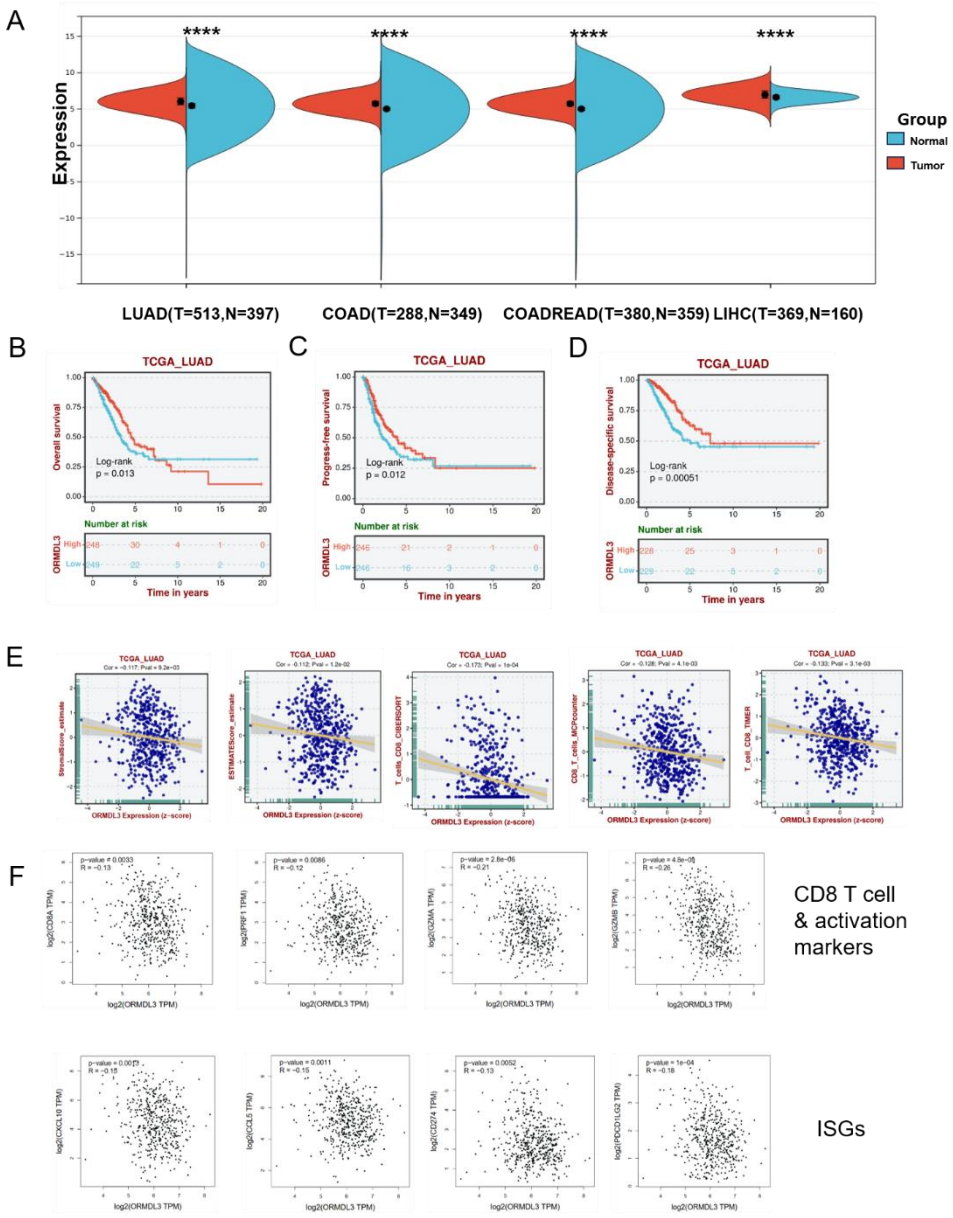

Supplementary Figure 6. ORMDL3 expression is associated with poor survival and reduced immune cell infiltration and ISGs.

(A) ORMDL3 expression between tumor and adjacent normal tissues in The Cancer Genome Atlas(TCGA) pan-cancer cohorts. **(B to D)** Association of ORMDL3 level with overall survival(OS),progression free survival(PFS) and disease-specific survival(DSS) in TCGA-LUAD. **(E)** Correlation among ORMDL3 expression with stromalscore and CD8T cell infiltration in

769 LUAD cohort from TCGA datasets. **(F)** Correlation among ORMDL3 expression with CD8
770 activation markers: CD8A, PRF1, GZMA, GZMB and ISG: CCL5, CXCL10, CD274 and
771 PDCD1LG2 in The Cancer Genome Atlas (TCGA) pan-cancer cohorts form the TIMER2.0
772 database.
773

Supplementary Figure 7

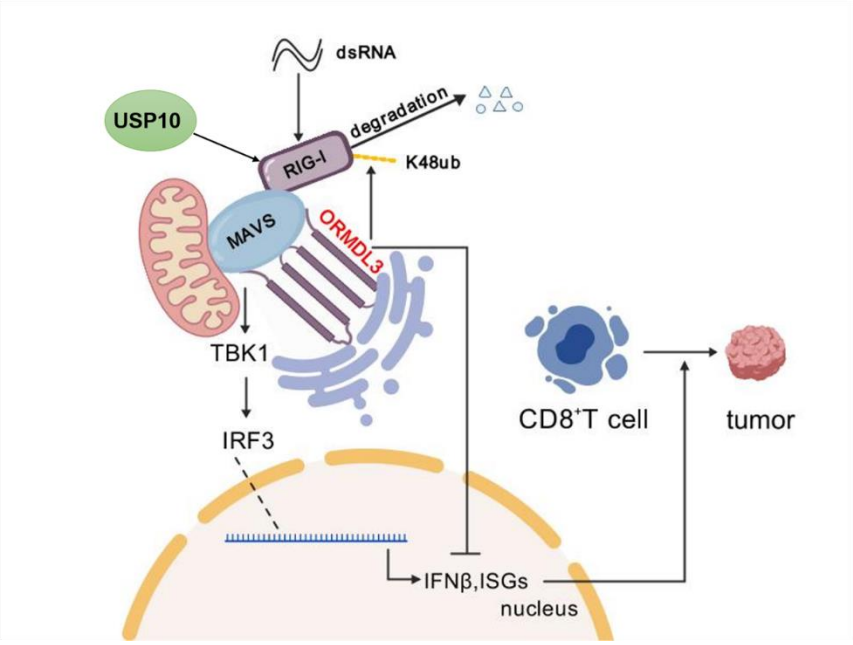

774

775 **Supplementary Figure 7. Schematic show that ORMDL3 promotes the degradation of RIG-I**

776 **and attenuates IFN in cancer.**

777

778

779

780

781

782

783

784

785

786

787 **Supplementary Table 1. Primers for qPCR. Related to Materials and Methods.**

788

Gene name	Primer sequences (from 5' to 3')
18S Forward	GTAACCCGTTGAACCCCATT
18S Reverse	CCATCCAATCGGTAGTAGCG
IFNB1 Forward	GTCAGAGTGGAAATCCTAAG
IFNB1 Reverse	ACAGCATCTGCTGGTTGAAG
CCL5 Forward	ATCCTCATTGCTACTGCCCTC
CCL5 Reverse	GCCACTGGTGTAGAAATACTCC
CXCL10 Forward	GCTCTACTGAGGTGCTATGTTC
CXCL10 Reverse	GGAGGATGGCAGTGGAAGTC
ISG54 Forward	GGAGGGAGAAAACTCCTTGGA
ISG54 Reverse	GGCCAGTAGGTTGCACATTGT
TNF Forward	AGTGAAGTGCTGGCAACCAC
TNF Reverse	GAGGAAGGCCTAAGGTCCAC
IL-6 Forward	GCCTTCTTGGGACTGATGCT
IL-6 Reverse	CTGCAAGTGCATCATCGTTGT
ORMDL1 Forward	TGACCAGGGTAAAGCAAGGC
ORMDL1 Reverse	CCGAACACCATGTAGTTGTGG
ORMDL2 Forward	GTGGCACACAGCGAAGTAAAC
ORMDL2 Reverse	TGCAGCAATCCTACCAAGATG
ORMDL3 Forward	AACACGCGGGTGATGAACAG
ORMDL3 Reverse	AGGGACACTCACAAACGGGA
RIG-I Forward	CTGCAAGCCTTCCAGGATTATAT
RIG-I Reverse	TCTGATCTGAGAAGGCATTCCA
ORMDL3 SNP sequence Forward	GCGACAGCGAGACTCCATCTCC
ORMDL3 SNP sequence Reverse	TCAGAACCAAGGCCCTTATTAG
USP10 Forward	CCCTCTCCTGGAATAGGGCA
USP10 Reverse	TCTCGGCAAAGTGTCACTGG
mice QPCR sequence	
β-Actin Forward	AGTGTGACGTTGACATCCGT
β-Actin Reverse	GCAGCTCAGTAACAGTCCGC
Ifnb1 Forward	ATGAGTGGTGGTTGCAGGC
Ifnb1 Reverse	TGACCTTTCAAATGCAGTAGATTCA
Ccl5 Forward	AGGACTCTGAGACAGCACAT
Ccl5 Reverse	GCAGTGAGGATGATGGTGAG
Cxcl10 Forward	TCAGGCTCGTCAGTTCTAAGTT
Cxcl10 Reverse	GATGGTGGTTAAGTTCGTGCTT
il-6 Forward	TAGTCCTTCCTACCCCAATTTCC
il-6 Reverse	TTGGTCCTTAGCCACTCCTTC
tnf Forward	AAGCCTGTAGCCCACGTCGT
tnf Reverse	GGCACCACTAGTTGGTTGTCTT
Ormdl3 Forward	CCAACCTTATCCACAACCTGG
Ormdl3 Reverse	GACCCCGTAGTCCATCTGC

789

790 **Reference**

791 1 Dalskov L, Gad H H, Hartmann R. Viral recognition and the antiviral interferon

792 response. *The EMBO Journal* **42**, doi:10.15252/embj.2022112907 (2023).

793 2 McNab F, Mayer-Barber K, Sher A *et al.* Type I interferons in infectious disease. *Nat*

794 *Rev Immunol* **15**, 87-103, doi:10.1038/nri3787 (2015).

795 3 Zitvogel L, Galluzzi L, Kepp O *et al.* Type I interferons in anticancer immunity. *Nature*

796 *Reviews Immunology* **15**, 405-414, doi:10.1038/nri3845 (2015).

797 4 Holicek P, Guilbaud E, Klapp V *et al.* Type I interferon and cancer. *Immunological*

798 *Reviews* **321**, 115-127, doi:10.1111/imr.13272 (2023).

799 5 Gajewski T F, Fuertes M B, Woo S-R. Innate immune sensing of cancer: clues from

800 an identified role for type I IFNs. *Cancer Immunology, Immunotherapy* **61**, 1343-1347,

801 doi:10.1007/s00262-012-1305-6 (2012).

802 6 Yang X, Zhang X, Fu May L *et al.* Targeting the Tumor Microenvironment with

803 Interferon-β Bridges Innate and Adaptive Immune Responses. *Cancer Cell* **25**, 37-48,

804 doi:10.1016/j.ccr.2013.12.004 (2014).

805 7 Zitvogel L, Galluzzi L, Smyth Mark J *et al.* Mechanism of Action of Conventional and

806 Targeted Anticancer Therapies: Reinstating Immunosurveillance. *Immunity* **39**, 74-88,

807 doi:10.1016/j.immuni.2013.06.014 (2013).

808 8 Spaapen R M, Leung M Y K, Fuertes M B *et al.* Therapeutic Activity of High-Dose

809 Intratumoral IFN-β Requires Direct Effect on the Tumor Vasculature. *The Journal of*

810 *Immunology* **193**, 4254-4260, doi:10.4049/jimmunol.1401109 (2014).

811 9 Goubau D, Deddouche S, Reis e Sousa C. Cytosolic sensing of viruses. *Immunity* **38**,
812 855-869, doi:10.1016/j.immuni.2013.05.007 (2013).
813 10 Hartmann G. Nucleic Acid Immunity. *Adv Immunol* **133**, 121-169,
814 doi:10.1016/bs.ai.2016.11.001 (2017).
815 11 Cheon H, Borden E C, Stark G R. Interferons and Their Stimulated Genes in the
816 Tumor Microenvironment. *Seminars in Oncology* **41**, 156-173,
817 doi:10.1053/j.seminoncol.2014.02.002 (2014).
818 12 Chiappinelli Katherine B, Strissel Pamela L, Desrichard A *et al.* Inhibiting DNA
819 Methylation Causes an Interferon Response in Cancer via dsRNA Including
820 Endogenous Retroviruses. *Cell* **162**, 974-986, doi:10.1016/j.cell.2015.07.011 (2015).
821 13 Roulois D, Loo Yau H, Singhania R *et al.* DNA-Demethylating Agents Target
822 Colorectal Cancer Cells by Inducing Viral Mimicry by Endogenous Transcripts. *Cell*
823 **162**, 961-973, doi:10.1016/j.cell.2015.07.056 (2015).
824 14 Guo H, Korolowicz K E, Iyer R P *et al.* Antiviral Efficacy and Host Innate Immunity
825 Associated with SB 9200 Treatment in the Woodchuck Model of Chronic Hepatitis B.
826 *PLoS One* **11**, doi:10.1371/journal.pone.0161313 (2016).
827 15 Jones M, Cunningham M E, Wing P *et al.* SB 9200, a novel agonist of innate
828 immunity, shows potent antiviral activity against resistant HCV variants. *Journal of*
829 *Medical Virology* **89**, 1620-1628, doi:10.1002/jmv.24809 (2017).
830 16 Middleton M R, Wermke M, Calvo E *et al.* Phase I/II, multicenter, open-label study of
831 intratumoral/intralesional administration of the retinoic acid–inducible gene I (RIG-I)
832 activator MK-4621 in patients with advanced or recurrent tumors. *Annals of Oncology*

833 **29**, doi:10.1093/annonc/mdy424.016 (2018).

834 17 Gack M U, Shin Y C, Joo C-H *et al.* TRIM25 RING-finger E3 ubiquitin ligase is
835 essential for RIG-I-mediated antiviral activity. *Nature* **446**, 916-920,
836 doi:10.1038/nature05732 (2007).

837 18 Yan J, Li Q, Mao A P *et al.* TRIM4 modulates type I interferon induction and cellular
838 antiviral response by targeting RIG-I for K63-linked ubiquitination. *J Mol Cell Biol* **6**,
839 154-163, doi:10.1093/jmcb/mju005 (2014).

840 19 Kuniyoshi K, Takeuchi O, Pandey S *et al.* Pivotal role of RNA-binding E3 ubiquitin
841 ligase MEX3C in RIG-I–mediated antiviral innate immunity. **111**, 5646-5651,
842 doi:doi:10.1073/pnas.1401674111 (2014).

843 20 Gao D, Yang Y K, Wang R P *et al.* REUL is a novel E3 ubiquitin ligase and stimulator
844 of retinoic-acid-inducible gene-I. *PLoS One* **4**, e5760,
845 doi:10.1371/journal.pone.0005760 (2009).

846 21 Oshiumi‡ H, M M, Shigetsugu Hatakeyama§ , and Tsukasa Seya‡. Riplet/RNF135, a
847 RING Finger Protein, Ubiquitinates RIG-I to Promote Interferon-ℕ Induction during the
848 Early Phase of Viral Infection. *THE JOURNAL OF BIOLOGICAL CHEMISTRY* **284**,
849 doi:10.1074/jbc.M804259200 (2009).

850 22 Chen W, Han C, Xie B *et al.* Induction of Siglec-G by RNA viruses inhibits the innate
851 immune response by promoting RIG-I degradation. *Cell* **152**, 467-478,
852 doi:10.1016/j.cell.2013.01.011 (2013).

853 23 Wang W, Jiang M, Liu S *et al.* RNF122 suppresses antiviral type I interferon
854 production by targeting RIG-I CARDs to mediate RIG-I degradation. *Proc Natl Acad*

855 *Sci U S A* **113**, 9581-9586, doi:10.1073/pnas.1604277113 (2016).

856 24 Kei-ichiro Arimoto* H T, Takayuki Hishiki*, Hideyuki Konishi*, Takashi Fujita†, and
857 Kunitada Shimotohno*‡. <arimoto-et-al-2007-negative-regulation-of-the-rig-i-
858 signaling-by-the-ubiquitin-ligase-rnf125.pdf>. (2007).

859 25 Zhao C, Jia M, Song H *et al.* The E3 Ubiquitin Ligase TRIM40 Attenuates Antiviral
860 Immune Responses by Targeting MDA5 and RIG-I. *Cell Rep* **21**, 1613-1623,
861 doi:10.1016/j.celrep.2017.10.020 (2017).

862 26 Cui J, Song Y, Li Y *et al.* USP3 inhibits type I interferon signaling by deubiquitinating
863 RIG-I-like receptors. *Cell Res* **24**, 400-416, doi:10.1038/cr.2013.170 (2014).

864 27 Fan Y, Mao R, Yu Y *et al.* USP21 negatively regulates antiviral response by acting as
865 a RIG-I deubiquitinase. *J Exp Med* **211**, 313-328, doi:10.1084/jem.20122844 (2014).

866 28 Wang L, Zhao W, Zhang M *et al.* USP4 positively regulates RIG-I-mediated antiviral
867 response through deubiquitination and stabilization of RIG-I. *J Virol* **87**, 4507-4515,
868 doi:10.1128/JVI.00031-13 (2013).

869 29 Pauli E-K, Chan Y K, Davis M E *et al.* The Ubiquitin-Specific Protease USP15
870 Promotes RIG-I–Mediated Antiviral Signaling by Deubiquitylating TRIM25. *Science*
871 *Signaling* **7**, doi:10.1126/scisignal.2004577 (2014).

872 30 Zhang Y M. Orosomucoid-like protein 3, rhinovirus and asthma. *World J Crit Care*
873 *Med* **10**, 170-182, doi:10.5492/wjccm.v10.i5.170 (2021).

874 31 Ha S G, Ge X N, Bahaie N S *et al.* ORMDL3 promotes eosinophil trafficking and
875 activation via regulation of integrins and CD48. *Nat Commun* **4**, 2479,
876 doi:10.1038/ncomms3479 (2013).

877 32 McGovern D P, Gardet A, Torkvist L *et al.* Genome-wide association identifies
878 multiple ulcerative colitis susceptibility loci. *Nat Genet* **42**, 332-337,
879 doi:10.1038/ng.549 (2010).
880 33 Qiu R, Zhang H, Zhao H *et al.* Genetic variants on 17q21 are associated with
881 ankylosing spondylitis susceptibility and severity in a Chinese Han population.
882 *Scandinavian Journal of Rheumatology* **42**, 469-472,
883 doi:10.3109/03009742.2013.786755 (2013).
884 34 Ma X, Qiu R, Dang J *et al.* ORMDL3 contributes to the risk of atherosclerosis in
885 Chinese Han population and mediates oxidized low-density lipoprotein-induced
886 autophagy in endothelial cells. *Sci Rep* **5**, 17194, doi:10.1038/srep17194 (2015).
887 35 Kurreeman F A, Stahl E A, Okada Y *et al.* Use of a multiethnic approach to identify
888 rheumatoid- arthritis-susceptibility loci, 1p36 and 17q12. *Am J Hum Genet* **90**, 524-
889 532, doi:10.1016/j.ajhg.2012.01.010 (2012).
890 36 Hitomi Y, Kojima K, Kawashima M *et al.* Identification of the functional variant driving
891 ORMDL3 and GSDMB expression in human chromosome 17q12-21 in primary biliary
892 cholangitis. *Scientific Reports* **7**, doi:10.1038/s41598-017-03067-3 (2017).
893 37 Xiang B, Deng C, Qiu F *et al.* Single cell sequencing analysis identifies genetics-
894 modulated ORMDL3+ cholangiocytes having higher metabolic effects on primary
895 biliary cholangitis. *Journal of Nanobiotechnology* **19**, doi:10.1186/s12951-021-01154-
896 2 (2021).
897 38 Moffatt M F, Kabesch M, Liang L *et al.* Genetic variants regulating ORMDL3
898 expression contribute to the risk of childhood asthma. *Nature* **448**, 470-473,

899 doi:10.1038/nature06014 (2007).

900 39 Caliskan M, Bochkov Y A, Kreiner-Moller E *et al.* Rhinovirus wheezing illness and
901 genetic risk of childhood-onset asthma. *N Engl J Med* **368**, 1398-1407,
902 doi:10.1056/NEJMoa1211592 (2013).

903 40 Rehwinkel J, Gack M U. RIG-I-like receptors: their regulation and roles in RNA
904 sensing. *Nat Rev Immunol* **20**, 537-551, doi:10.1038/s41577-020-0288-3 (2020).

905 41 Li S, Xie T, Liu P *et al.* Structural insights into the assembly and substrate selectivity
906 of human SPT-ORMDL3 complex. *Nat Struct Mol Biol* **28**, 249-257,
907 doi:10.1038/s41594-020-00553-7 (2021).

908 42 Jin R, Yuan W X, Xu H G *et al.* Characterization of a novel isoform of the human
909 ORMDL3 gene. *Cell Tissue Res* **346**, 203-208, doi:10.1007/s00441-011-1261-z
910 (2011).

911 43 Wang H, Yin J, Gu X *et al.* Immune Regulator Retinoic Acid-Inducible Gene I (RIG-I)
912 in the Pathogenesis of Cardiovascular Disease. *FRONTIERS IN IMMUNOLOGY* **13**,
913 doi:10.3389/fimmu.2022.893204 (2022).

914 44 Fitzgerald K A, McWhirter S M, Faia K L *et al.* IKKε and TBK1 are essential
915 components of the IRF3 signaling pathway. *Nature Immunology* **4**, 491-496,
916 doi:10.1038/ni921 (2003).

917 45 Zhao K, Zhang Q, Li X *et al.* Cytoplasmic STAT4 Promotes Antiviral Type I IFN
918 Production by Blocking CHIP-Mediated Degradation of RIG-I. *J Immunol* **196**, 1209-
919 1217, doi:10.4049/jimmunol.1501224 (2016).

920 46 Carreras-Sureda A, Cantero-Recasens G, Rubio-Moscardo F *et al.* ORMDL3

921 modulates store-operated calcium entry and lymphocyte activation. *Hum Mol Genet*
922 **22**, 519-530, doi:10.1093/hmg/dds450 (2013).
923 47 Cantero-Recasens G, Fandos C, Rubio-Moscardo F *et al.* The asthma-associated
924 ORMDL3 gene product regulates endoplasmic reticulum-mediated calcium signaling
925 and cellular stress. *Hum Mol Genet* **19**, 111-121, doi:10.1093/hmg/ddp471 (2010).
926
927
928
929
930